

Prediction and Modeling of the San Francisco Bay area transients using Interferometric Synthetic Aperture Radar

Sreeja Nag

Abstract

Interferometry relies on the constructive and destructive interference of electromagnetic waves from sources at two or more vantage points at different times. For InSAR, the interference pattern is constructed from two complex-valued synthetic aperture radar images, and interferometry is the study of the phase difference between two images which can be inverted to give surface topography and ground displacements. Synthetic aperture radar (SAR) data were collected over the San Francisco Bay Area by the European Space Agency (ESA) using the ERS-1 and ERS-2 spacecraft from 1992 to 2000 in 46 epochs. The data are time series of surface displacements for different latitude-longitude values. Two sections: The Santa Clara Valley and the Loma Preita region have been chosen for specific analysis due to the proven transient phenomena observed in both the regions. Identification of seasonal variations, DC offsets and separating them from tectonically caused variations is done using functional analysis and principal component analysis. Frequency related components are separated, frequency content evaluated using Empirical Mode Decomposition and the seasonal modes assessed. Modeling of the Loma Preita section is initiated via Kalman Filtering using a 2 fault model, one reverse and one strike slip near the SAF zone. Green's functions are calculated using Okada's technique and random walk probabilistic parameters determined. The slip histories on faults thus found via the Network Inversion Filter are dependent only on tectonics and results may be checked with those from the previous tools.

Key words: InSAR, San Francisco Bay Area, Loma Preita, Santa Clara, Principal Component Analysis, Empirical Mode Decomposition, Hilbert Spectrum, Kalman Filtering, Network Inversion Filter.

TRANSIENT ANALYSIS OF INTERFEROMETRIC SAR DATA

I thank Dr. Roland Burgmann at the University of California, Berkeley, for providing me with the dataset, the idea used in this project and his consistent guidance on the techniques I used.

Sreeja Nag

May 2009

The time series obtained from InSAR is very valuable in showing the variation of displacement over long periods of time and thus slowly varying transient phenomena. Examples of such processes with respect to the San Francisco Bay area are:

1. Seasonal hydrologic, land subsidence processes (e.g., Schmidt, D. A., and R. Bürgmann (2003), Time dependent land uplift and subsidence in the Santa Clara valley, California, from a large InSAR data set, *Journal of Geophysical Research*, 108, doi:10.1029/2002JB002267.)
2. Time dependent landslide motion (in the Berkeley Hills, but also east of San Jose) that appear to accelerate depending on pore-pressure variations (e.g., Hilley, G. E., R. Bürgmann, A. Ferretti, F. Novali, and F. Rocca (2004), Dynamics of slow-moving landslides from permanent scatterer analysis, *Science*, 304, 1952-1955.)
3. Transient fault slip events on creeping faults in the region including the Hayward, Calaveras and San Andreas faults (we know there was a Feb. 1996 slip event on the southernmost Hayward fault as well as slip events on the San Andreas at the very edge of the data set we are looking at, but do not know if there is more time dependence to slip on these faults otherwise).
4. A very slowly decaying late-stage postseismic relaxation from the 1989 Loma Prieta earthquake (e.g., Segall, P., R. Bürgmann, and M. Matthews (2000), Time dependent deformation following the 1989 Loma Prieta earthquake, *Journal of Geophysical Research*, 105, 5615-5634.). There may well be other time-varying aspects to the surface deformation and/or complexities to the processes mentioned that the data may or may not reveal.

InSAR has been used to model subsidence, seismic relaxation and volcanic deformation ever since it was conceived. As candidate sites for the first two, our aim is to concentrate on 2 regions of the Bay Area – the Santa Clara Valley region and the Loma Prieta region (discussed in detail later). Identification of transients is done via: Principal component Analysis, Functional Fitting and Empirical Mode Decomposition. We intend to separate out the time series in different components and modes depending on the property that the

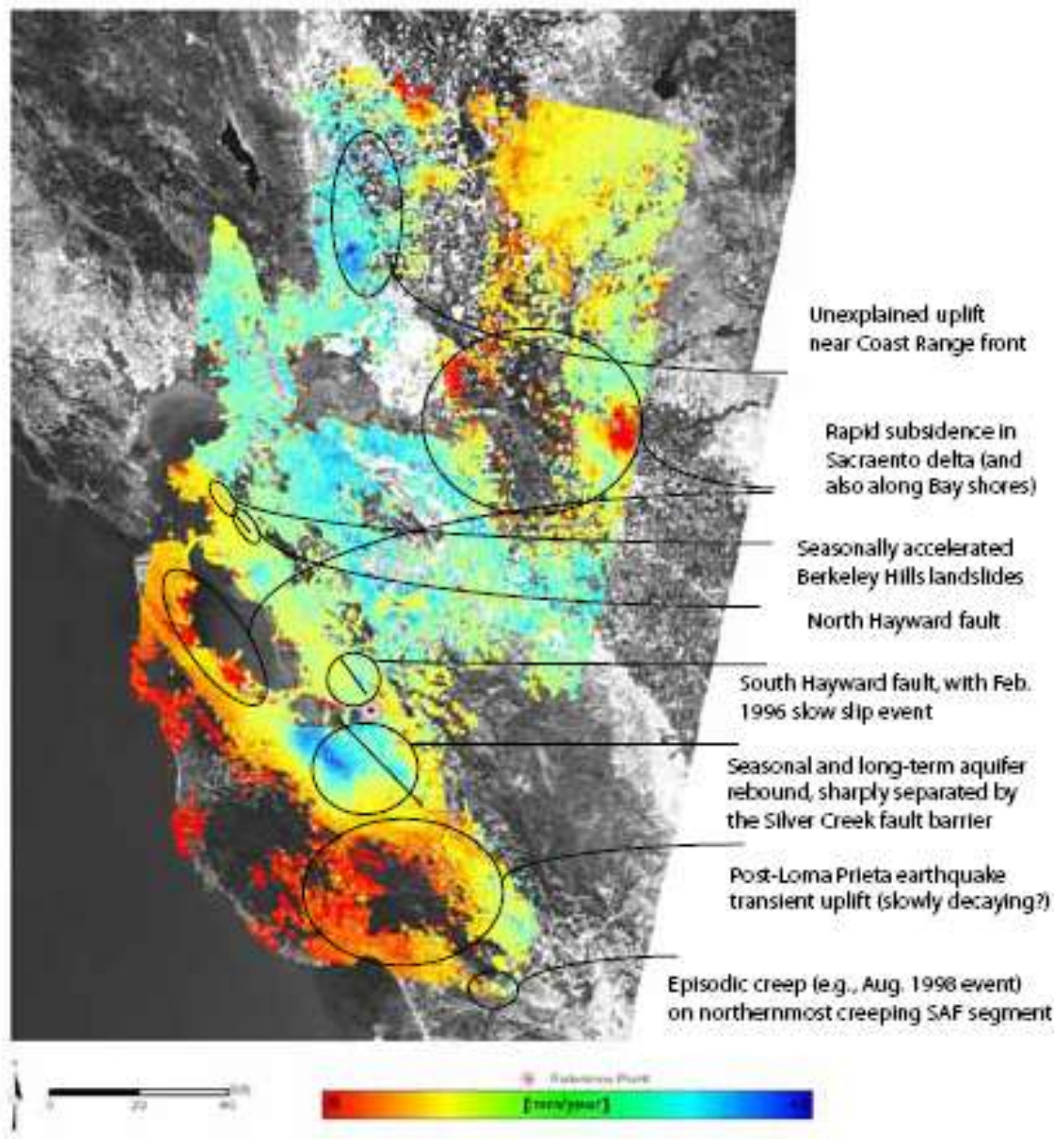


Figure 6a: Annotated map of the San Francisco Bay Area showing the various transient positions occurring and their spatial locations. Figure courtesy PS Technique - Sar data processing Final Report Date: 04/06/2008 Tele-Rilevamento Europa.

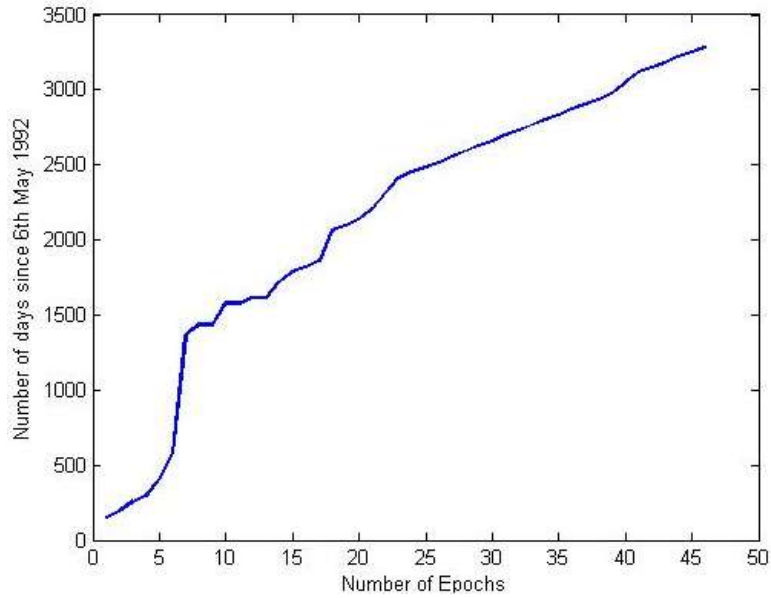


Figure 6b: Number of days vs the epochs at which the satellite took its readings

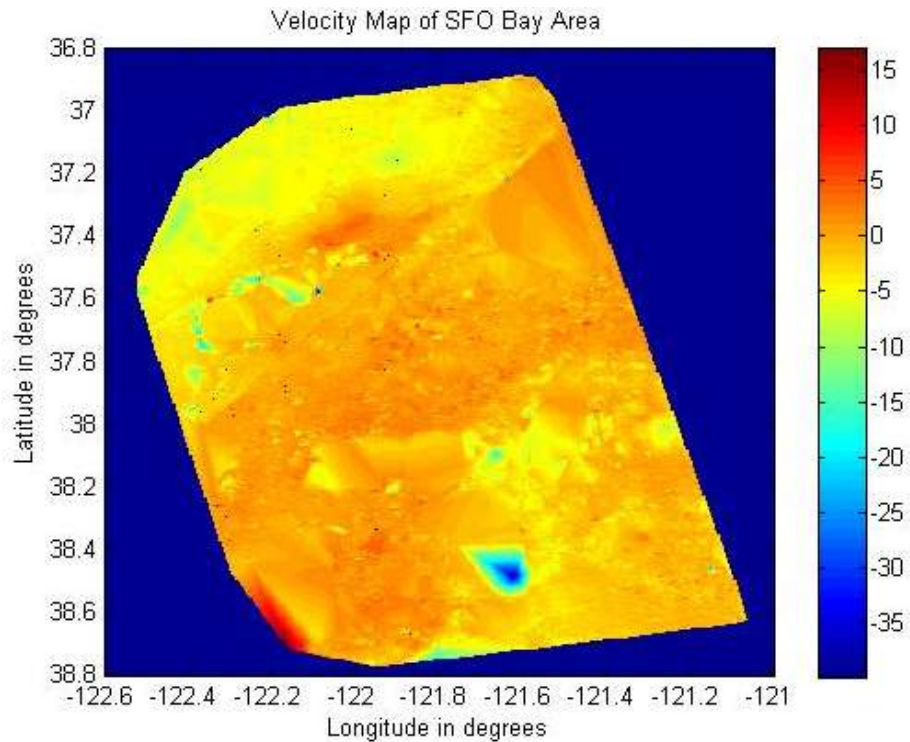


Figure 7: Velocity field of the San Francisco Bay area found by interpolation from the scattered data available. The uninterpolated version is superimposed on the map in Figure 6. The units are in mm/year.

technique concentrates upon. According to the interpretations made by the same, we will model the region's tectonics using the Network Inversion Filter. The previous approaches directly explore the data for "real" time dependent components without knowledge or assumptions of what the underlying process is. We want to find "real" time dependent deformation features and resolve their spatio-temporal distribution as best as we can from a massive data set of noisy and sparse time series data. GPS results for some of the processes are available to check for correlation with our InSAR results.

Synthetic aperture radar (SAR) data were collected over the San Francisco Bay Area by the European Space Agency (ESA) using the ERS-1 and ERS-2 spacecraft. We chose to limit the number of interferograms used in the analysis to those with small perpendicular baselines (<200 m) to ensure that errors imposed by topography remain small. Interferograms are produced using the Repeat Orbit Interferometry Package (ROI PAC) developed at the Jet Propulsion Laboratory and the California Institute of Technology (JPL/Caltech). SAR data are processed using 8 looks in range and 40 looks in azimuth resulting in a pixel width of roughly 150 m. A weighted power spectral density filter and an adaptive filter are applied to each interferogram [Goldstein and Werner, 1998]. Processing parameters were chosen to counter temporal decorrelation in those interferograms spanning several years while maximizing resolution. [11] Topography is removed from each interferogram using a 30 m U.S. Geological Survey (USGS) digital elevation model (DEM) and an evaluation of the elevation model suggests that imposed errors are negligible. A DEM of the Bay Area derived from the Shuttle Radar Topography Mapping (SRTM) mission was not available at the time that the interferograms were processed. Upon the recent release of the SRTM data a comparison was performed with the USGS DEM. A 50-km-wavelength signal with maximum peak-to-trough amplitude of 2.7 m was found in the residual between elevation models for the flat, urban regions of the bay area. However, the analysis of tandem ERS InSAR data (1-day interferograms) suggests that this anomalous signal originates from the SRTM data set. A 2.7 m elevation change would translate to 1 mm in range change for a

perpendicular baseline of 100 m. Therefore errors imposed on the interferograms from the USGS DEM are likely to be <1 mm.

The final processed data comprises: Universal Mercator coordinates of each data point location, standard deviation of the average velocity of the point, phase coherence measure of the same (as defined in *Ferretti et al. 2000 paper* and *Colesanti et al., 2002*), mean range-change rate with respect to reference pixel and the range/displacement time series at each epoch from May 1992 through 2000.

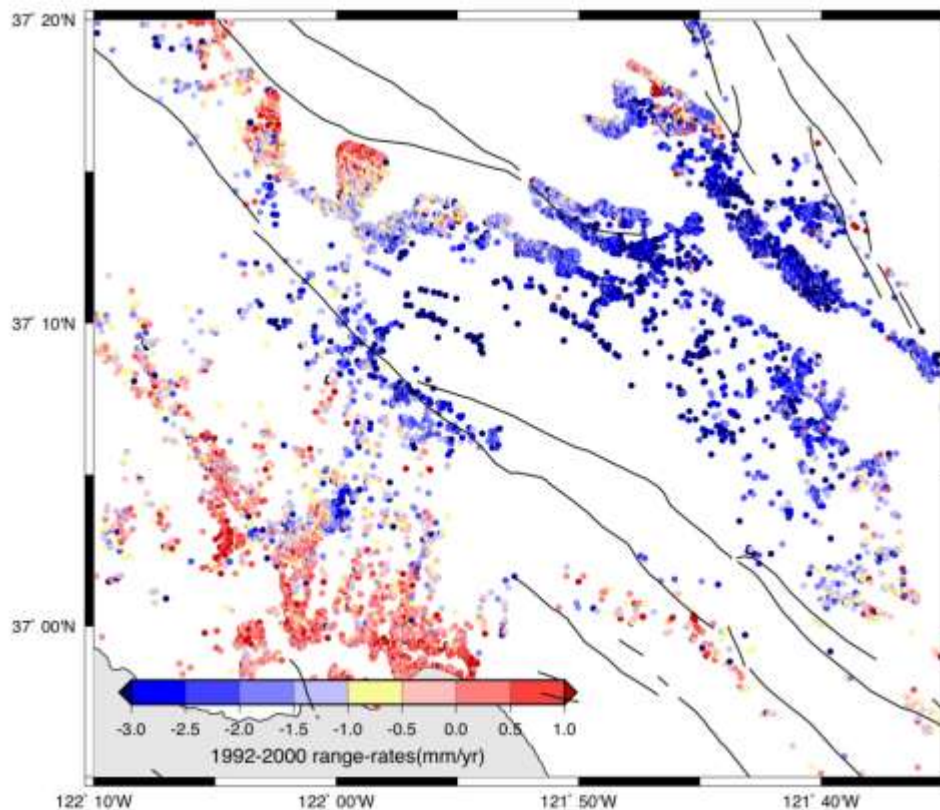


Figure 8a: Loma Prieta region (-122.66 to -121.75 degrees east, 36.916 to 37.33 degrees north) – plot of the GPS velocity field scatter with points on Quaternary substrate (that may experience non-tectonic, seasonal deformation) and the contribution of background horizontal motions removed.

Data specifications are as follows:

Range = -20 to 20 mm

2.7 lakh points

Time spacing = 30-60 days (6th May 1992 – 9th December 2000)

No of time samples = 46

Resolution = 1.5 km

Area dimension = 19072 sq. km

No. of PS points = 217561

8 looks in range, 40 looks in azimuth

Repeat orbit ~ 35 days

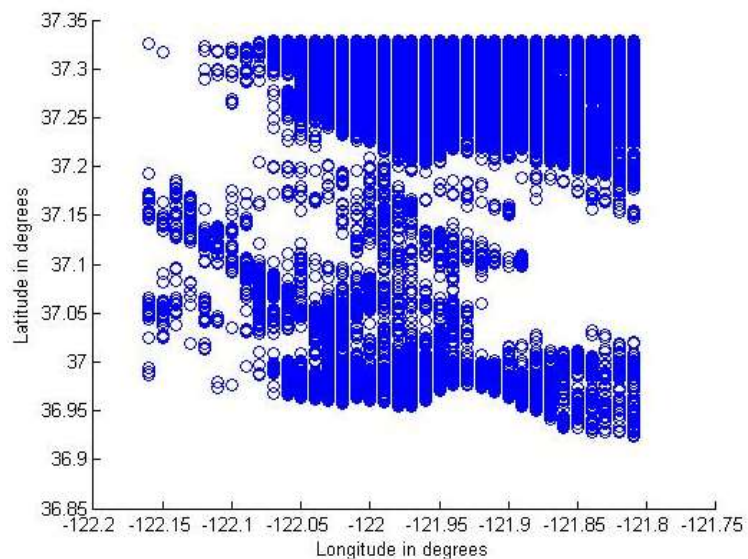


Figure 8b: Scatter plot of the InSAR PS data points within the Loma Prieta region chosen for our analysis.

Since there were above 10000 points we downsampled the data by averaging the values within boxes of 0.1 degrees by 0.1 degrees.

Loma Prieta postsismic model

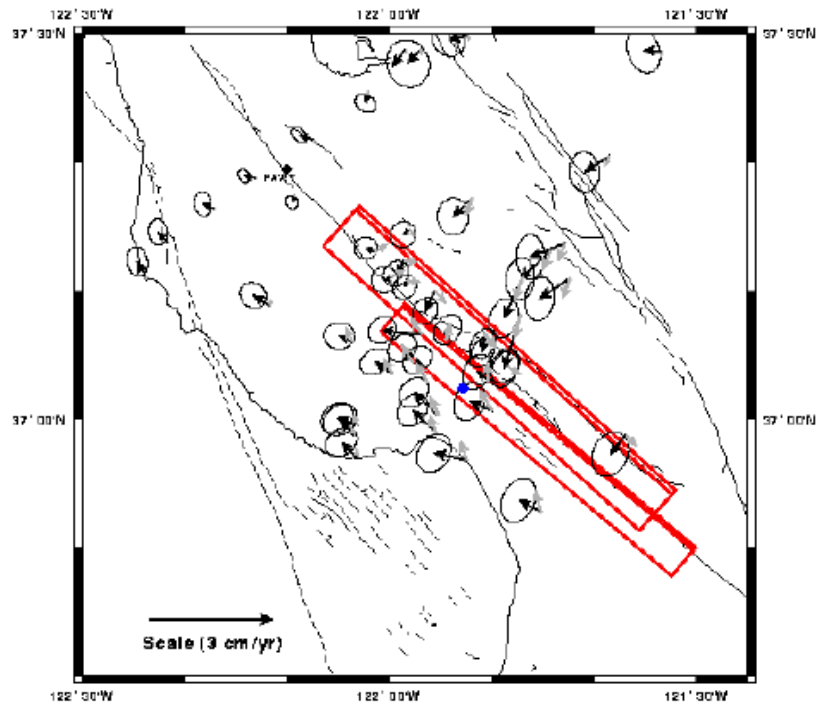


Figure 8c: Postseismic velocity vectors

Figures courtesy Burgmann et al, JGR 1997

SAF slip rate = 20-35 mm/year, right lateral

This value along with the fields shown in the above figures justify the values in our InSAR dataset

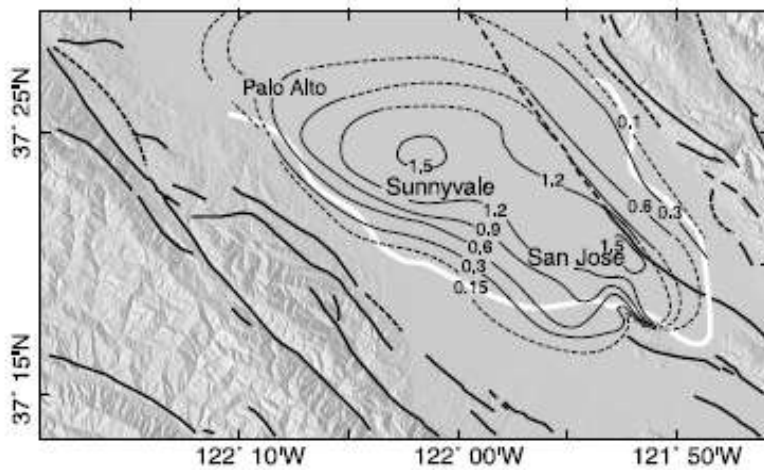
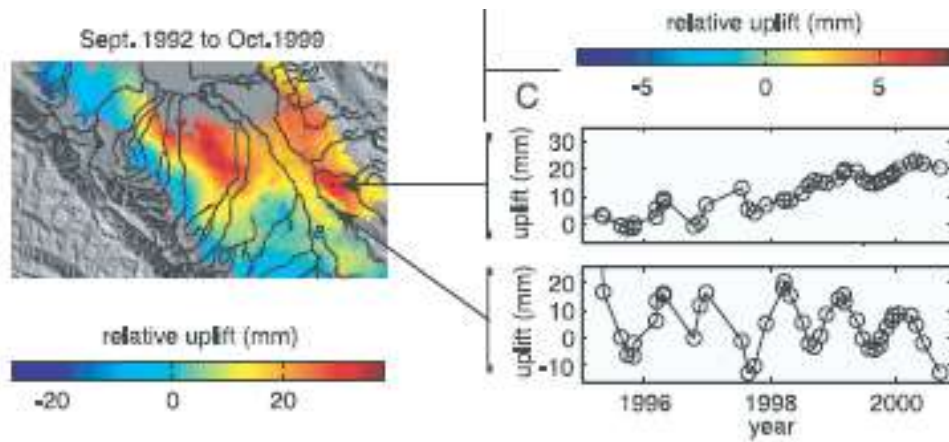


Figure 9a: Land subsidence observed from 1934 to 1960 reproduced from Poland and Ireland [1988, Figure 19] using GPS data collected by the National Geodetic Survey. Subsidence contours (thin lines, irregular intervals) are in units of m, dashed where poorly controlled. Santa Clara valley region we used ranged from -121.833 to -122.33 degrees east and 37.25 to 37.5 degrees north. Figures Courtesy Burgmann and Schmidt, JGR 2002.

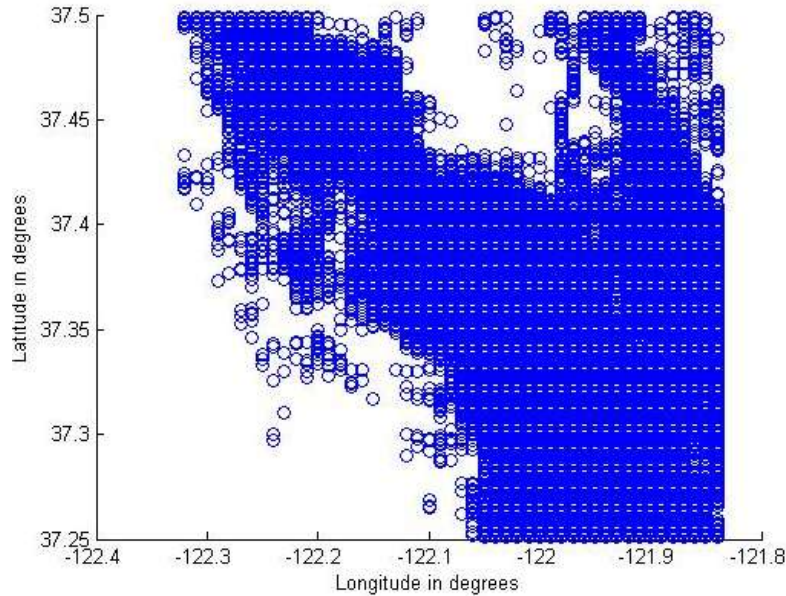


Figure 9b: Scatter plot of the InSAR PS data points within the Santa Clara region chosen for our analysis. Since there were above 10000 points we downsampled the data by averaging the values within boxes of 0.1 degrees by 0.1 degrees.

3.1. PRINCIPAL COMPONENT ANALYSIS

PCA is a very good first approach for this analysis as it considers the "modes" of spatial and temporally patterns in deformation data that can be related to individual deformation processes. For some of processes we are interested in exploring/detecting in our own data, this seems applicable; including landslide motion, coastal sediment settling, first-order effects from groundwater level changes, seasonal land subsidence, and postseismic relaxation.

3.1.1. Theory and applicability to triangulation networks

Savage 1994 resolved the observed deformation of a trilateration network into a superposition of modes by means of principal component analysis. Let L_i be the length of a segment averaged over time and L_{ij} the length of the i th segment at the j th time. If we define $D_{ij} = L_{ij} - L_i$, then

$$D_{ij} = \sum_{k=1}^N A_{ik} C_k(t_j)$$

where k = mode number

A_{ik} = participation of A_i th segment in the k th mode

C_k = participation of the C_j th time slot in the k th mode

One technique to do this is by finding the best fit curve to the first mode is evaluated and stripped off from the data, the curve for the second mode fitted, and so on. The total error is calculated as the sum of squared residuals and is given as:

$$SSR = \sum_{i=1}^n \sum_{j=1}^m (D_{ij} - \sum_{p=1}^k A_{ip} C_p(t_j))^2$$

The paper found linear dependence of the first mode of the temporal factor with respect to time and sinusoidal variation in the spatial factor with respect to azimuth. Thus it could not identify any long-term coherent deformation pattern other than a linear trend. Typical geodetic measurements of deformation consist of repeated surveys of a particular geodetic network. Such deformation data can be interpreted as a consequence of one or more self-coherent sources by means of principal component analysis. A self-coherent source is defined as any source that produces deformation that is time and space separable. Principal component analysis then gives the time and space factors that characterize the deformation attributed to each self-coherent source. Geodetic measurements of deformation at Long Valley caldera provide two examples of the application of principal component analysis. A 40-line trilateration network surrounding the caldera was surveyed in midsummer 1983, 1984, 1985, 1986, and 1987. Principal component analysis indicates that the observed deformation can be represented by a single coherent source. The time dependence for that source displays a rapid rate of deformation in 1983-1984 followed by less rapid but uniform rate in the 1984-1987 interval. The spatial factor seems consistent with expansion of a magma chamber beneath the caldera plus some shallow right-lateral slip on a vertical fault in the south moat of the caldera. An independent principal component analysis of the 1982, 1983, 1984, 1985, 1986, and 1987 leveling across the caldera requires two self-coherent sources to explain the deformation. The deformation pattern produced by the larger of these two sources appears to be roughly consistent with that found from the trilateration data. The

deformation due to the second source is a nearly uniform tilt in the uplift profile. Presumably, that tilt is simply an artifact of systematic error in the leveling.

Clearly, a big challenge is that various noise source can also be systematically correlated in space and time. PCA also known as orthogonal functional analysis is no more than singular value decomposition given by [Aubrey and Emery, 24A]. PCA is mathematically defined as an orthogonal linear transformation that transforms the data to a new coordinate system such that the greatest variance by any projection of the data comes to lie on the first coordinate (called the first principal component), the second greatest variance on the second coordinate, and so on. PCA is theoretically the optimum transform for a given data in least square terms. PCA can be used for dimensionality reduction in a data set by retaining those characteristics of the data set that contribute most to its variance, by keeping lower-order principal components and ignoring higher-order ones. However, depending on the application this may not always be the case.

3.1.2. Singular Value Decomposition

For a data matrix, \mathbf{X}^T , with zero empirical mean (the empirical mean of the distribution has been subtracted from the data set), where each row represents a different repetition of the experiment, and each column gives the results from a particular probe, the PCA transformation is given by:

$$\begin{aligned}\mathbf{Y}^T &= \mathbf{X}^T \mathbf{W} \\ &= \mathbf{V} \mathbf{\Sigma}\end{aligned}$$

where $\mathbf{V} \mathbf{\Sigma} \mathbf{W}^T$ is the singular value decomposition (svd) of \mathbf{X}^T . PCA has the distinction of being the optimal linear transformation for keeping the subspace that has largest variance. This advantage, however, comes at the price of greater computational requirement if compared, for example, to the discrete cosine transform. In our case, Y is the spatially dependent factor and X the temporally dependent, both orthogonal to each other and hence mutually independent.

3.1.3. Results and Interpretation for Loma Prieta

PCA successfully showed the expected spatial variation in the Loma Prieta region. As is seen from Figure 10c, the maximum amount of contribution comes from the first mode after which the modes oscillate about zero, provide negligible contribution and are similar to each other. Since the order of points in the scatter plot in Figure 8b is in ascending lat-long and not a particular azimuth, we plotted the parameter values interpolated onto a lat-long grid for better visualization of the results. The maximum contribution map is shown in Figure 10a. The NE corner sector has a relative downthrow with respect to the SW sector of the map and is three times the order of magnitude. The sectors are separated by the Loma Prieta fault shown in Figure **AB**. The results correlated perfectly with the GPS findings of the region in the scatter map of Figure 8a with respect to the location throws as well as the magnitude. The third mode hardly has a contribution and is anticorrelated with mode 1. The temporal parameter has similar contribution from the 5 modes plotted. All modes show a significant decrease in signal around epoch 15 which is about 4.5 years after the beginning of

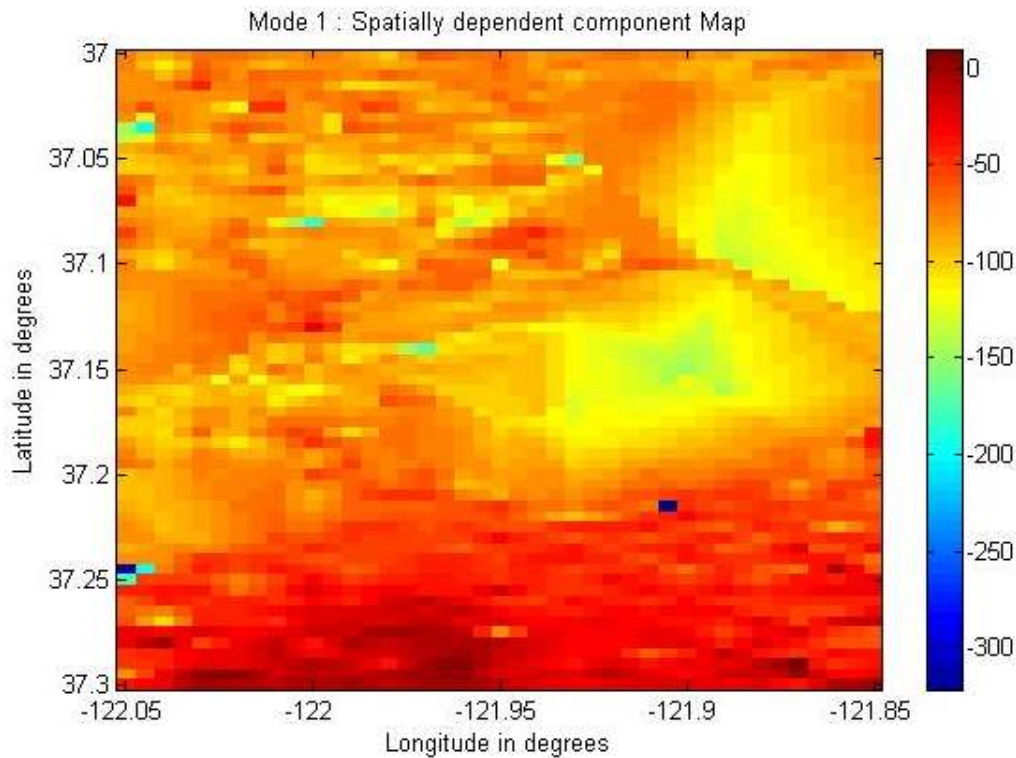


Figure 10a: Mode 1 of the spatial factor of Loma Prieta.

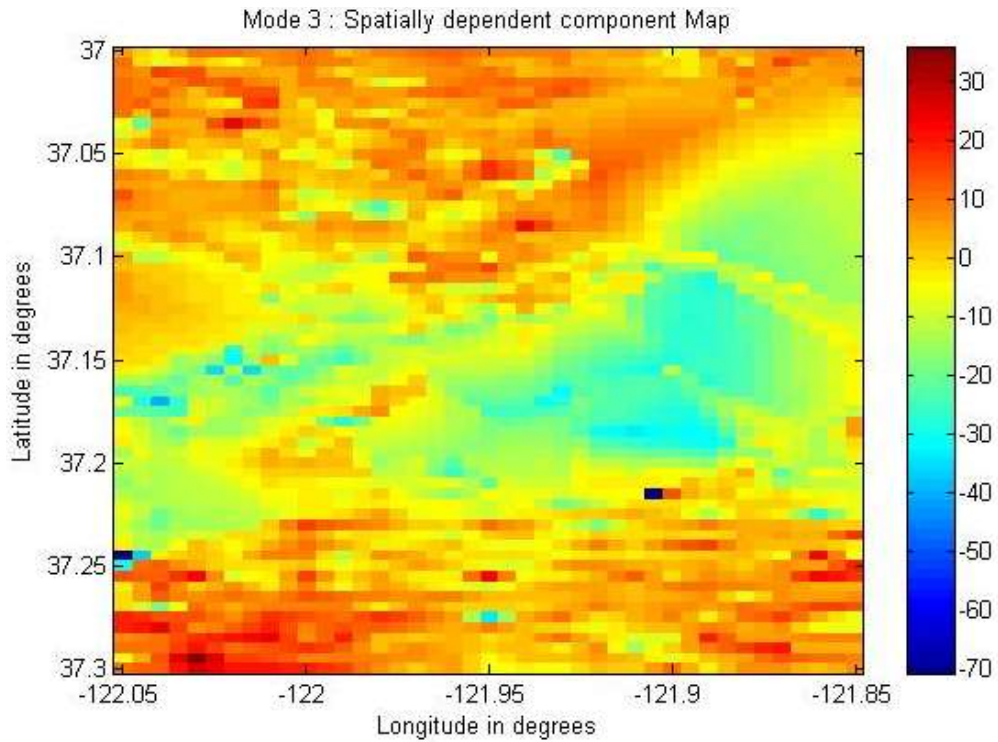


Figure 10b: Mode 3 of the spatial factor of Loma Prieta.

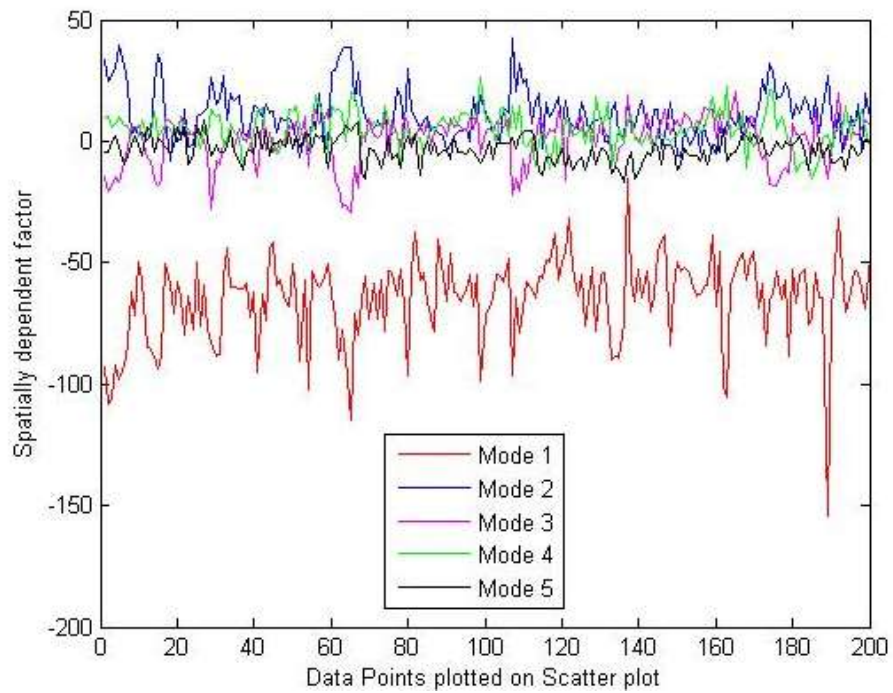


Figure 10c: Spatially dependent parameter with respect to data points on the scatter plot in Figure

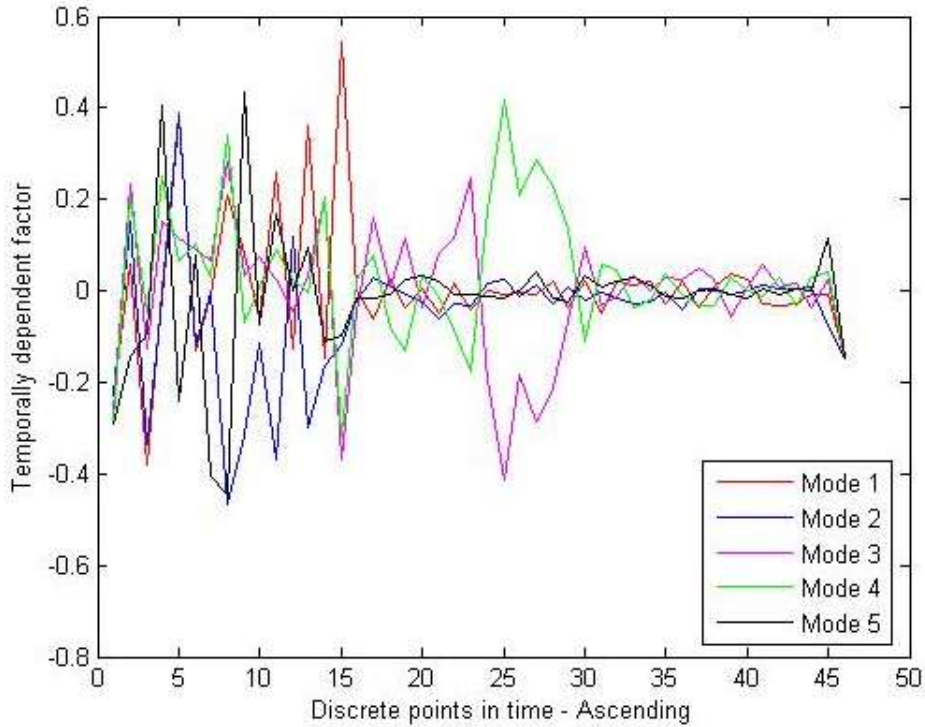


Figure 11: Temporal factor of Loma Prieta with respect to number of epochs (46 in 8 years)

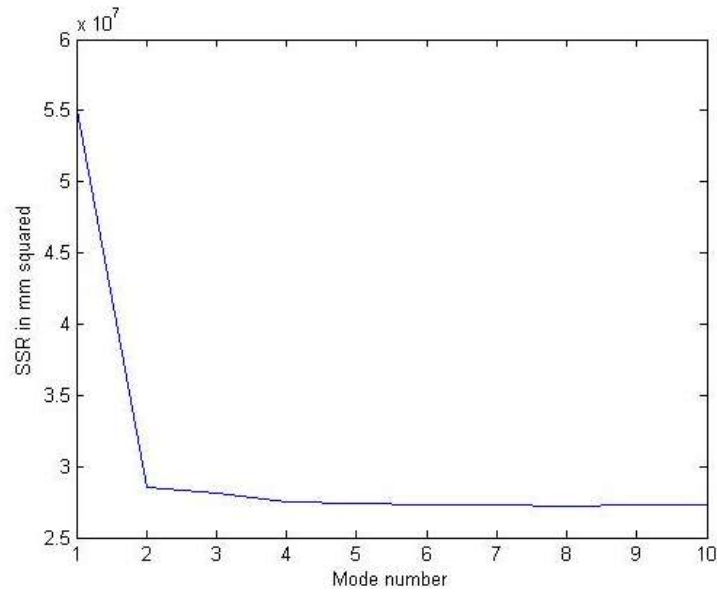


Figure 12: Sum of squared residuals of the Loma Prieta PCA Analysis

data collected and thus a bit over 6 years since the Loma Prieta earthquake. This could be interpreted as post-seismic relaxation. A functional analysis is done later to check for the same.

3.1.3. Results and Interpretation for Santa Clara

As was above, the maximum amount of contribution comes from the first mode after which the modes oscillate about zero, provide negligible contribution and are similar to each other. Since the order of points in the scatter plot in Figure 9b is in ascending lat-long and not a particular azimuth, we plotted the parameter values interpolated onto a lat-long grid for better visualization of the results. The maximum contribution map is shown in Figure 13a. It shows a clear partition of uplift in the SW and subsidence in the NE via a NW-SE trending lineage which we know from previous studies to be the position of the Silver Creek Fault.

Such a partitioning is seen in the GPS derived contours of Figure 8a too. The third mode hardly has a contribution and is anticorrelated with mode 1. The temporal parameter has similar contribution from the 5 modes plotted and does not give much information. This could be because the deformation with respect to time of the two sides of the partition are

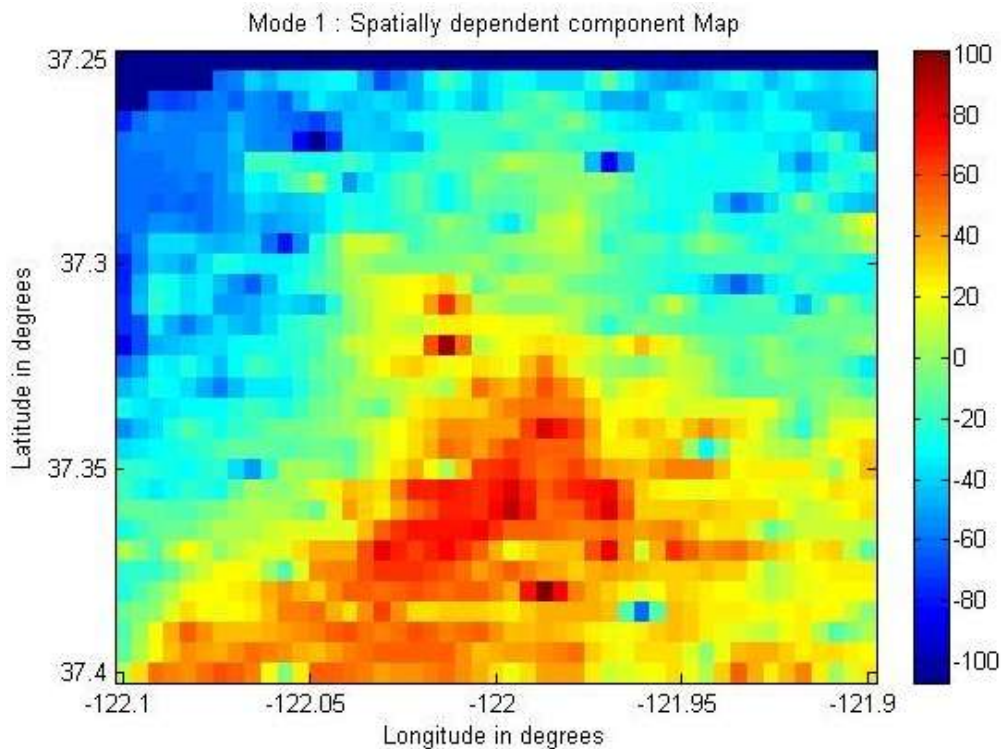


Figure 13a: Mode 1 of the spatial factor of Santa Clara

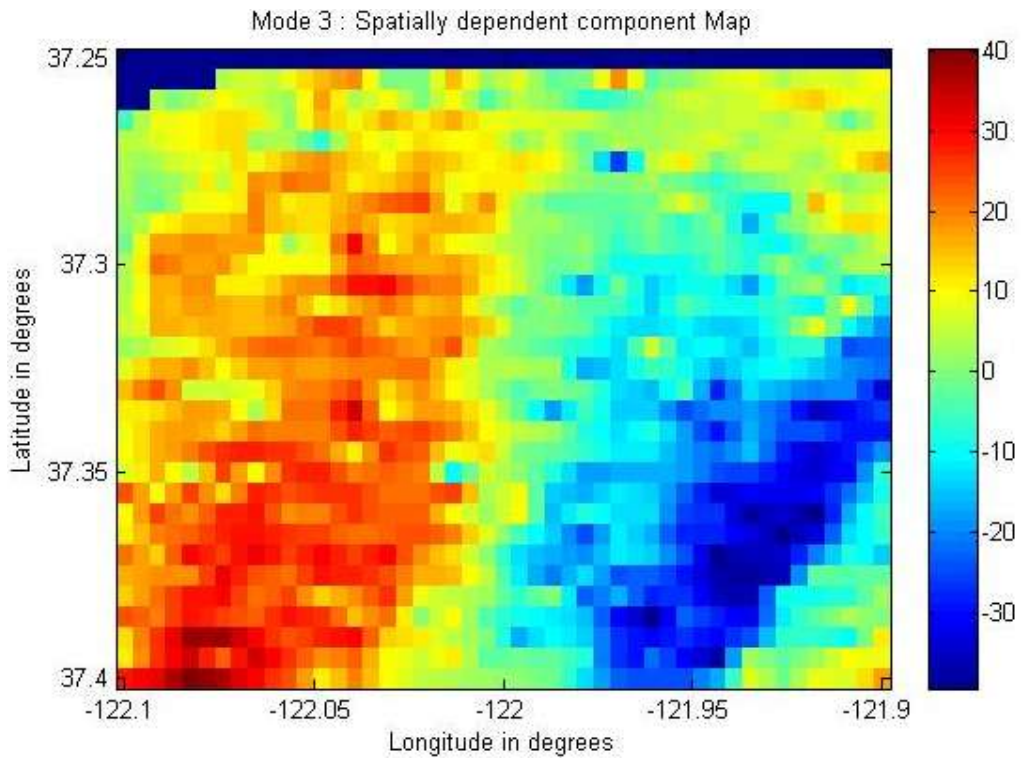


Figure 13b: Mode 3 of the spatial factor of Santa Clara

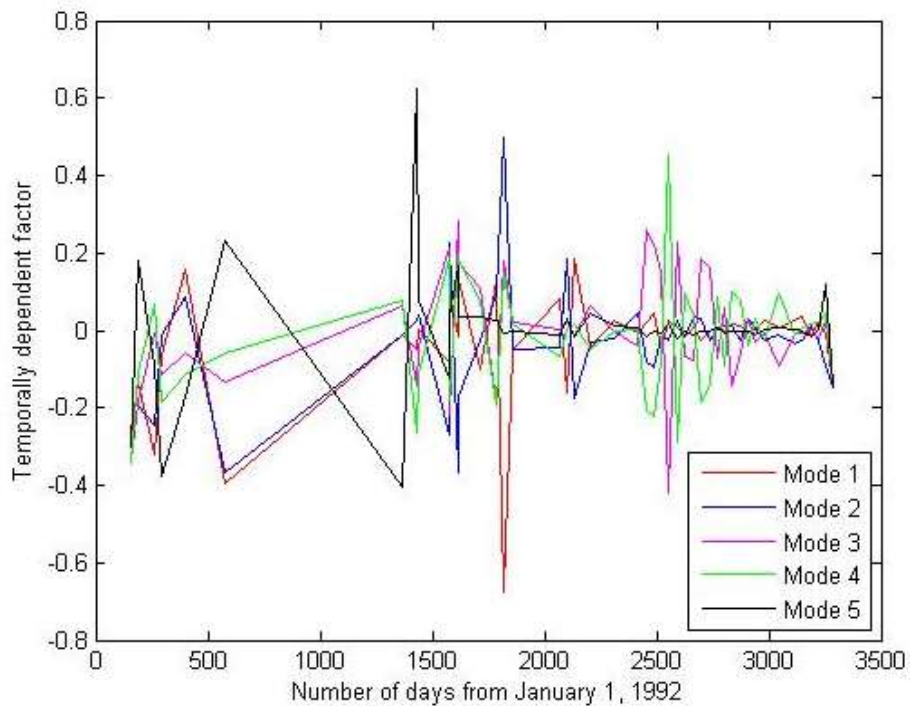


Figure 14: Temporal factor of Santa Clara with respect to number of epochs (46 in 8 years)

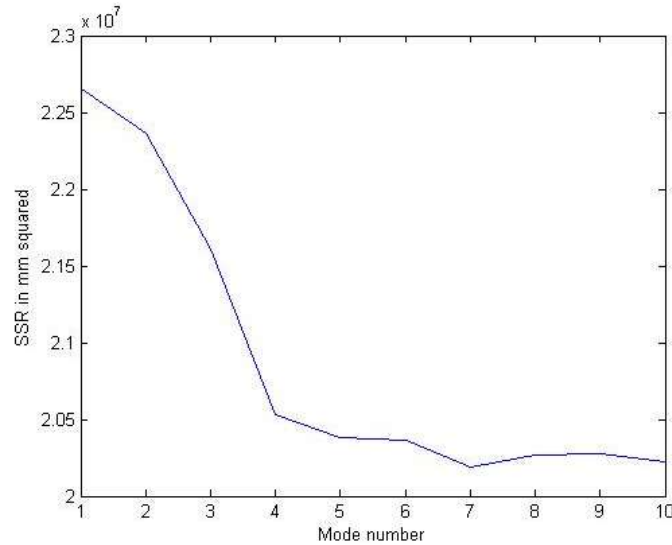


Figure 15: Sum of squared residuals of the Santa Clara PCA Analysis

quite different and hence when PCA is done on the entire area, it averages out. There are a large number of oscillations in the modes, though, which could be seasonal and functional analysis proves so later.

3.2. FUNCTIONAL FITTING

3.2.1. Theory and significance of the simple mathematical terms

Time series data can be simplified as a summation of simple functional components. Freed et al. 2006 were interested in the cumulative surface deformation for the 2-year period following the 2002 earthquake (November 2002 through November 2004). Using two complete years enables us to estimate and remove annual and semiannual signals within the GPS data. To constrain the temporal dependence and specially to understand the contribution of transients and seasonal factors, we model site positions as the sum of (1) a linear term representing secular elastic strain accumulation, (2) a logarithmic term representing postseismic deformation, (3) an annual and semiannual periodic term representing seasonal effects not modeled in the GPS data analysis, and (4) DC offsets due to equipment changes or problems at the site. The model equation is:

$$y = a*\sin(2*\pi*t) + b*\cos(2*\pi*t) + c*\exp(t/T) + d*t + e$$

where a, b, c, d, e and T are estimated by inverting the site position data y using least mean squares estimation. The logarithmic term in equation is a convenient means of parameterizing time-dependent postseismic deformation. Although the data can be well fit by this model, we do not ascribe a physical significance to the estimated model parameters or predictive power to the overall model. They use this approach only as a curve-fitting convenience to remove nontectonic effects (seasonal variations and DC offsets) and estimate displacement uncertainties.

We used a regression model to determine the coefficients. A regression model is a linear one when the model comprises a linear combination of the parameters, i.e.

$$f(x_i, \beta) = \sum_{j=1}^m \beta_j \phi_j(x_i)$$

where the coefficients, β_j , are functions of x_i , the input variable and β are the coefficients to be determined. Letting

$$X_{ij} = \frac{\partial f(x_i, \beta)}{\partial \beta_j} = \phi_j(x_i).$$

We can then see that in that case the least square estimate (or estimator, if we are in the context of a random sample), β is given by

$$\hat{\beta} = (X^T X)^{-1} X^T \mathbf{y}$$

A different technique called orthogonal regression or total least squares model with either QR decomposition or SVD may also be used.

3.2.2. Results and Interpretation for Loma Prieta

The time series of PS point -121.75E, 37.141N – a region on surface above the Loma Prieta fault and functional fitted according to model equation on. The coefficients inverted for have values A = -1.1605, B = -0.4033, C = 7.4925, D = -0.0172, E = -0.1691. Evidently, C

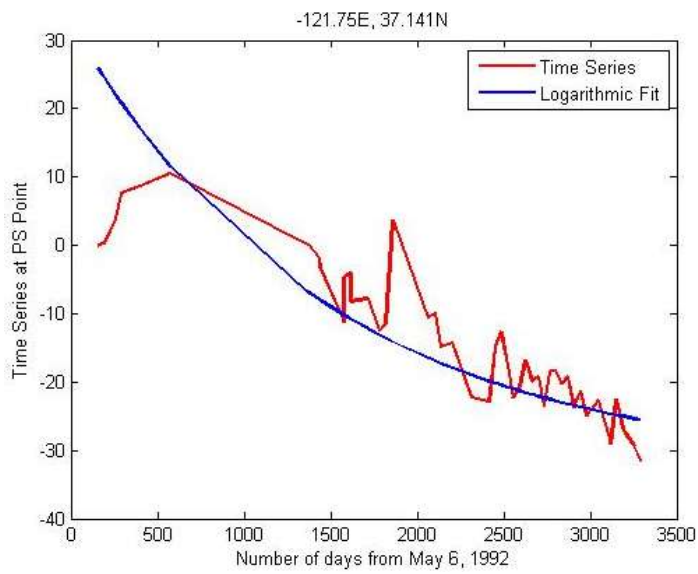
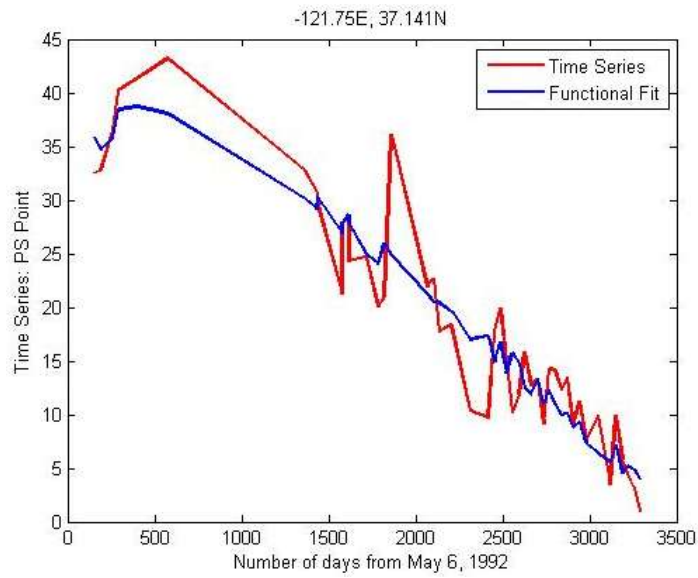


Figure 16a: Functional fit according to model equation on the time series of PS point st -121.75E, 37.141N – a region on surface above the Loma Prieta fault. Figure 16b: Pure log curve fitted to the time series.

i.e. the logarithmic coefficient has the maximum contribution significantly greater than the others. We thus fitted a pure log curve to the time series to find T or the logarithmic relaxation factor according to the model equation. The value comes to be 4 years. This is in agreement with the relaxation time from our PCA analysis too and also strengthens the claim that this is a viscous seismic relaxation signal. In theory, such a decrease can be explained by either the viscous relaxation of a ductile (asthenospheric) layer underlying an elastic (lithospheric) plate, or by the downward propagation of aseismic slip along a lower crustal extension of the fault zone. It could be a fault creep as Shallow creep typically decays exponentially within a few years of the earthquake [Smith and Wyss, 1968; Bilham, 1989]. Continued monitoring of the transient deformation will provide valuable information about mechanisms of time-dependant deformation following a large earthquake and its effects on neighboring faults (SAF, Hayward, Calaveras, LP, etc).

3.2.2. Results and Interpretation for Santa Clara

Since the Santa Clara Valley and aquifer is partitioned around the Silver Creek Fault and show substantially different deformation patterns. To understand the time dependence for both the regions separately we picked one PS point -121.92E, 37.35N on the SW of the fault and one PS point st -12.84E, 37.39N on the SW of the fault. Functional fit according to model equation on the time series of the first gives $A = -69.0669$, $B = 2.6883$, $C = 14.6155$, $D = -0.0055$, $E = -0.1992$ and the second gives $A = -18.5137$, $B = 0.4915$, $C = 6.7686$, $D = -0.0097$, $E = -0.2025$. The figures are normalised forms. The dominant term very noticeably is A i.e. the sine term which confirms the strong seasonal character of this region albeit via uplift and subsidence in different sectors. The InSAR time series reveals an overall pattern of uplift since 1992 centered north of Sunnyvale. Most of this uplift occurs between 1992 and 1998. The reasons can be due to poroelastic response, inelastic deformation to groundwater pumping and/or aquifer expansion as discussed in *Bawden et al, Nature 2001* and *Schmidt and Burgmann, JGR 2002*. The south west part is strongly seasonal and a pure sin-cos curve can be fitted on it.

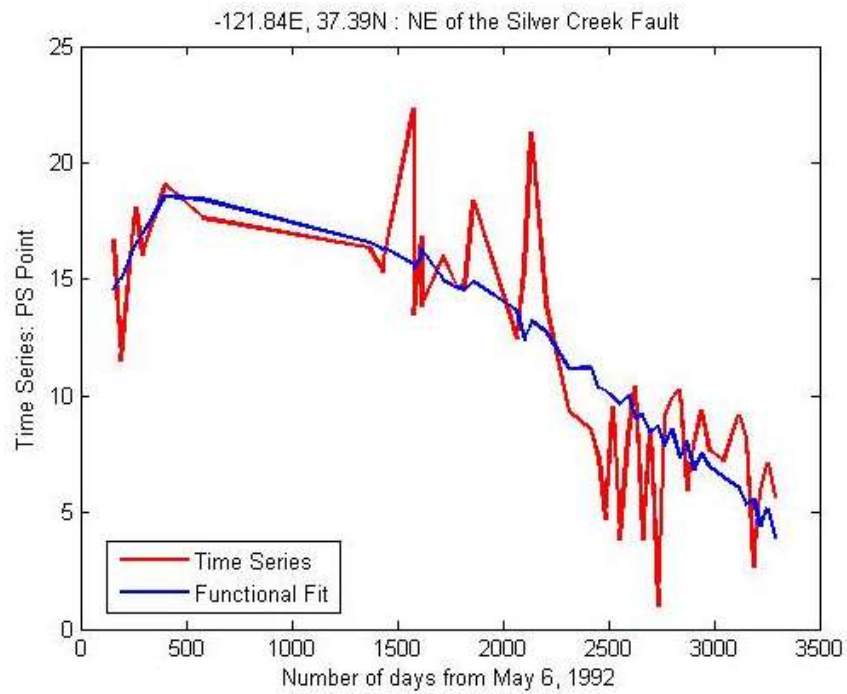
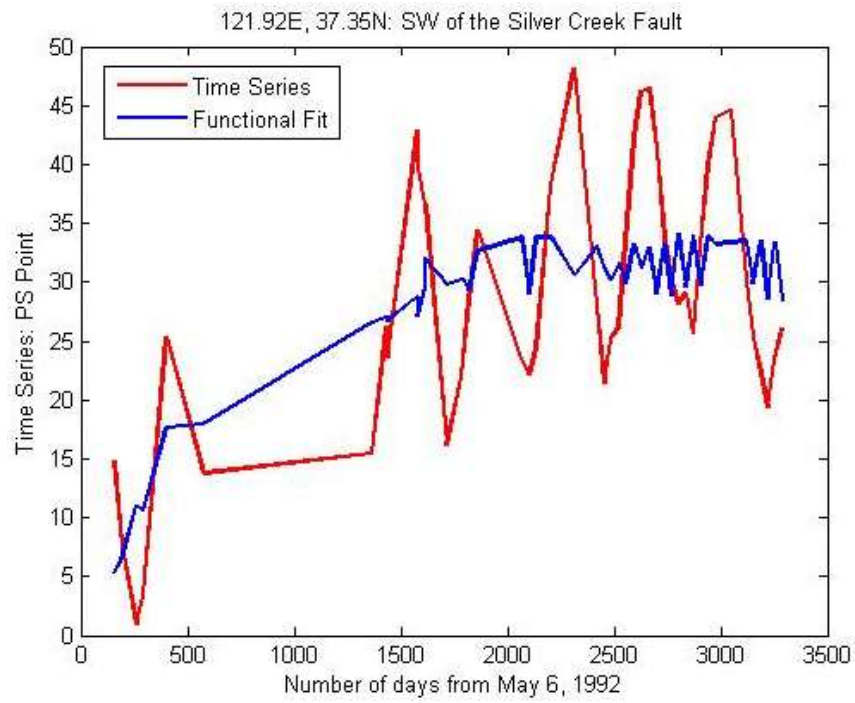


Figure 17a: Functional fit according to model equation on the time series of PS point st -121.92E, 37.35N on the SW of the Silver Creek Fault. Figure 17b: Functional fit according to model equation on the time series of PS point st -12184E, 37.39N on the SW of the Silver Creek Fault.

3.3. EMPIRICAL MODE DECOMPOSITION

Empirical Mode decomposition and Hilbert-Huang Transform are used for stationary signals to separate them out into various frequency components. These components are called intrinsic mode functions (IMFs) and the algorithm is called sifting. The essence is to identify the IMFs by time scales, which can be defined locally by the time lapse between two extrema of an oscillating mode or by time lapse between two zero crossings of such a mode. The idea then is to extract for each mode locally the highest frequency oscillations. To compute also the frequency behavior of each IMF in time, Huang proposed to use instantaneous frequency of each IMF. For this we have to ensure that each is symmetric with respect to its local mean, otherwise unwarranted fluctuations will occur. In some sense they can be seen as adaptive wavelet decompositions. Each IMF then replaces the detail signals. It is a fully data driven method and does not use any pre-determined filter or wavelet functions.

3.3.1. Theory and Algorithm

A new nonlinear technique, referred to as Empirical Mode Decomposition (EMD), has recently been pioneered by N.E. Huang et al. for adaptively representing nonstationary signals as sums of zero-mean components.

Given a signal $x(t)$, the effective algorithm of EMD can be summarized as follows :

1. identify all extrema of $x(t)$
2. interpolate between minima (resp. maxima) ending up with some envelope $e_{min}(t)$ (resp. $e_{max}(t)$)
3. compute the mean $m(t) = (e_{min}(t) + e_{max}(t)) / 2$
4. extract the detail $d(t) = x(t) - m(t)$
5. iterate on the residual $m(t)$

The above procedure has to be refined by a *sifting process* which amounts to first iterating steps 1 to 4 upon the detail signal $d(t)$, until this latter can be considered as zero-mean

according to some stopping criterion. Once this is achieved, the detail is referred to as an Intrinsic Mode Function (IMF), the corresponding residual is computed and step 5 applies. By construction, the number of extrema is decreased when going from one residual to the next, and the whole decomposition is guaranteed to be completed with a finite number of modes. The decomposition is based on the assumptions: (1) the signal has at least two extrema | one maximum and one minimum; (2) the characteristic time scale is defined by the time lapse between the extrema; and (3) if the data were totally devoid of extrema but contained only inflection points, then it can be differentiated once or more times to reveal the extrema. Final results can be obtained by integration(s) of the components. The essence of the method is to identify the intrinsic oscillatory modes by their characteristic time scales in the data empirically, and then decompose the data accordingly. A complication is that the envelope mean may be different from the true local mean for nonlinear data; consequently, some asymmetric wave forms can still exist no matter how many times the data are sifted. We have to accept this approximation.

3.3.2. Intrinsic Mode Functions and the Hilbert Spectrum

An intrinsic mode function (IMF) is a function that satisfies two conditions: (1) In the whole data set, the number of extrema and the number of zero crossings must either equal or differ at most by one; and (2) At any point, the mean value of the envelope defined by the local maxima and the envelope defined by the local minima is zero. Theoretically, there are infinitely many ways of defining the imaginary part, but the Hilbert transform provides a unique way of defining the imaginary part so that the result is an analytic function. Given the complex trace, the phase of the signal can be found and the instantaneous frequency is defined as differential of the phase with respect to time. The components of the EMD are usually physical, for the characteristic scales are physical. Nevertheless, this is not strictly true, for there are cases when a certain scale of a phenomenon is intermittent. Then, the decomposed component could contain two scales in one IMF component. Therefore, the

physical meaning of the decomposition comes only in the totality of the decomposed components in the Hilbert spectrum.

Having obtained the intrinsic mode function components, we will have no difficulties in applying the Hilbert transform to each component, and computing the instantaneous frequency. After performing the Hilbert transform on each IMF component, we can express the data in the following form:

$$X(t) = \sum_{j=1}^n a_j(t) \exp \left(i \int \omega_j(t) dt \right).$$

Here we have left out the residue, r_n , on purpose, for it is either a monotonic function, or a constant. The final representation may also be written as:

$$f(t) = \sum_{n=1}^N \psi_n + r_{N+1}$$

where $r_{N+1} = f_{N+1}$ is the residual.

Although the Hilbert transform can treat the monotonic trend as part of a longer oscillation, the energy involved in the residual trend could be overpowering. In consideration of the uncertainty of the longer trend, and in the interest of information contained in the other low-energy and higher-frequency components, the final non-IMF component should be left out. It, however, could be included, if physical considerations justify its inclusion. The above equation gives both the amplitude and the frequency of each component as functions of time. The same data if expanded in Fourier representation would be

$$X(t) = \sum_{j=1}^{\infty} a_j e^{i\omega_j t},$$

with both a_j and ω_j constants. The contrast between the two equations is clear: the IMF represents a generalized Fourier expansion. The variable amplitude and the instantaneous frequency have not only greatly improved the efficiency of the expansion, but also enabled the expansion to accommodate non-stationary data. With IMF expansion, the amplitude and the frequency modulations are also clearly separated. Thus, we have broken through the restriction of the constant amplitude and fixed-frequency Fourier expansion, and arrived at

a variable amplitude and frequency representation. This expression is numerical. If a function is more desired, an empirical polynomial expression can be easily derived from the IMFs. The integral equation also enables us to represent the amplitude and the instantaneous frequency as functions of time in a three-dimensional plot, in which the amplitude can be contoured on the frequency-time plane. This frequency-time distribution of the amplitude is designated as the Hilbert amplitude spectrum, $H(\omega; t)$, or simply Hilbert spectrum. If amplitude squared is more desirable commonly to represent energy density, then the squared values of amplitude can be substituted to produce the Hilbert energy spectrum just as well.

3.3.5. Results and Interpretation for Santa Clara

EMD is especially useful here because the region has proven regional character. Two time series were considered, again on two sides of the Silver Creek Fault. The decomposition extracts the high frequency or rapidly changing components first and then the next. Thus a range of frequencies can be explored one mode at a time. The Hilbert Spectrum shows a decrease in frequency values as the number of IMFs increase. For each mode, the time at which maximum amplitude content occurs and what frequency it occurs at is important in delineating the times at which that particular frequency mode becomes more dominant. Thus that seasonal phenomena can be constrained in time as well.

This technique could probably be more suitable for data with spectral/frequency aspects (such as the functional, wind, tide, and earthquake wave examples given) than the very sparse in time series we are exploring, in which we attempt to resolve time dependence that is coherent between enough points to be representing a real process. The simpler functional or principal component methods we previously discusses may be more directly applicable in that case. However, rather than just following potentially imperfect precedent, we are trying to explore the different responses of the data to all these techniques before settling on one analysis. We always have to keep in mind that it is a non-trivial problem to pull out the kind of transient processes we are interested in out of the data we have available.

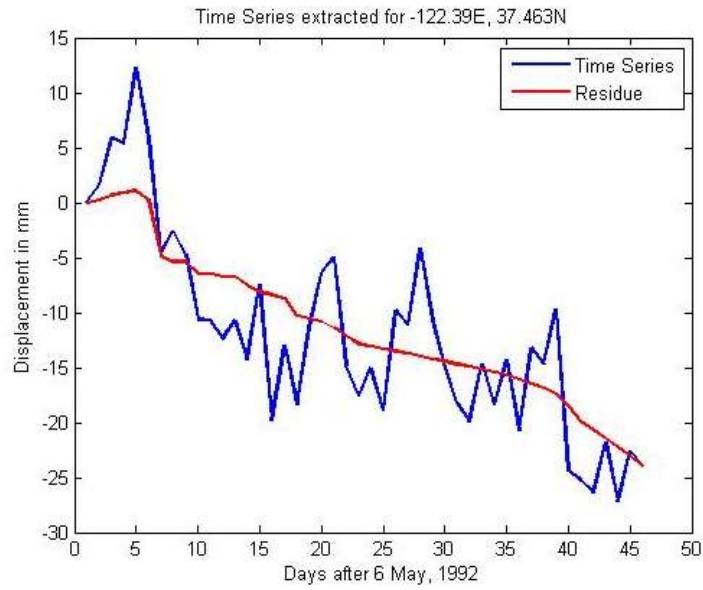


Figure 18a: Time series on the subsiding side of the Santa Clara Valley.

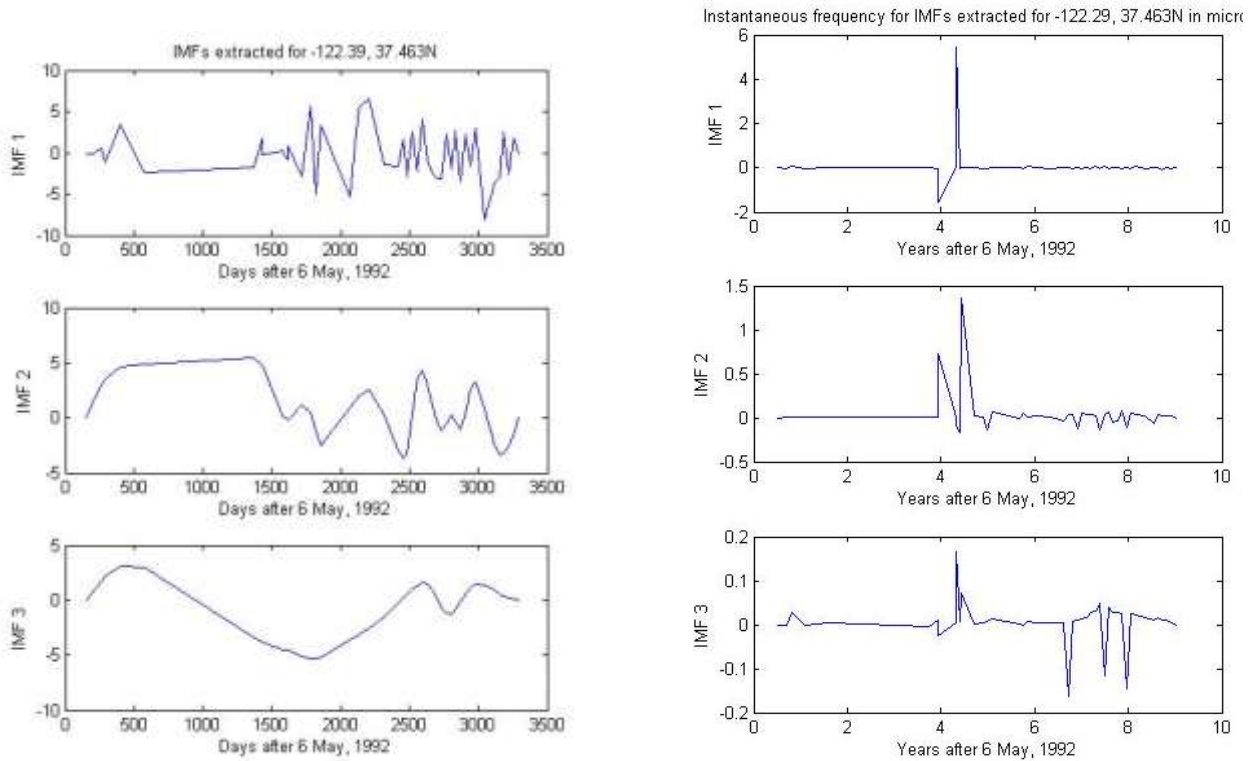


Figure 18b: IMFs extracted for the above time series and instantaneous frequency of the IMFs extracted.

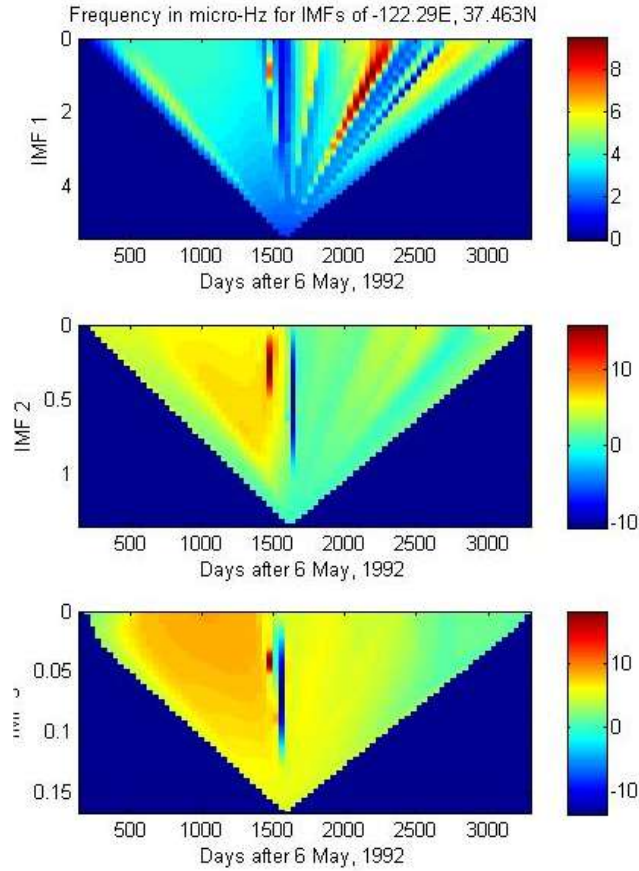


Figure 18c: Hilbert Spectrum for each of the IMFs extracted.

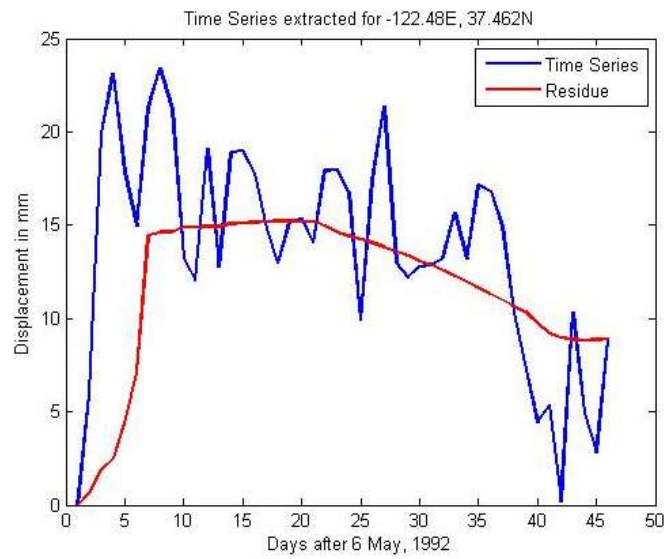


Figure 19a: Time series on the subsiding side of the Santa Clara Valley.

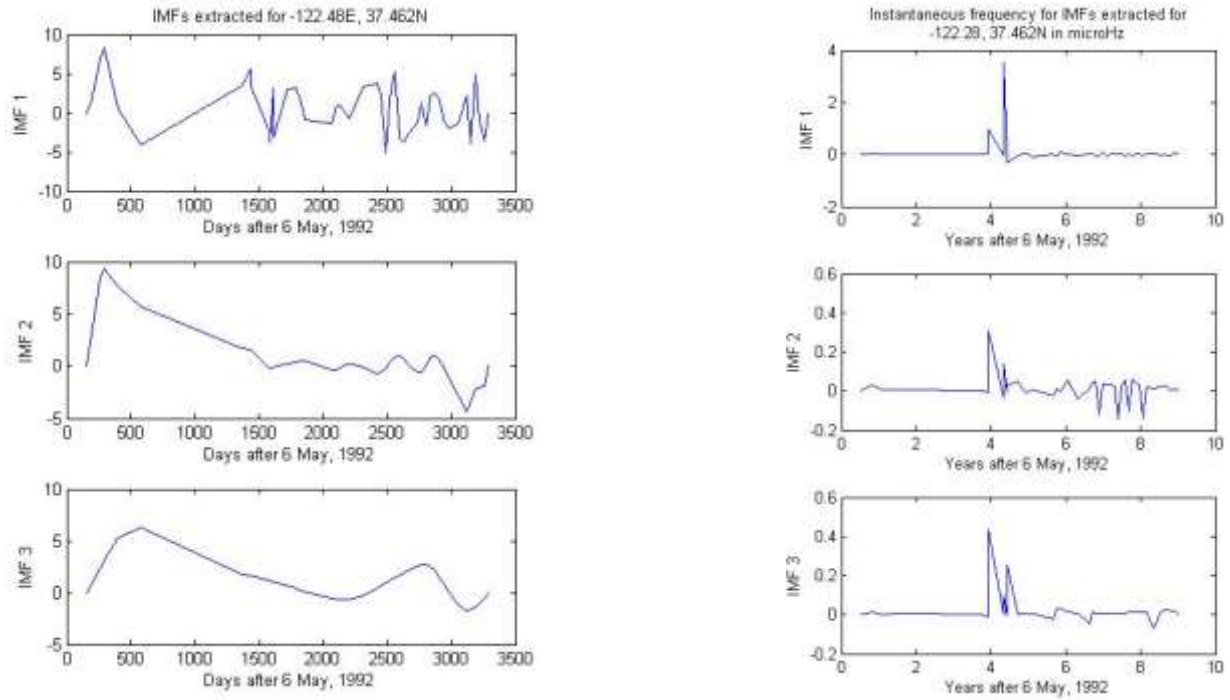


Figure 19b: IMFs extracted for the above time series and instantaneous frequency of the IMFs extracted.

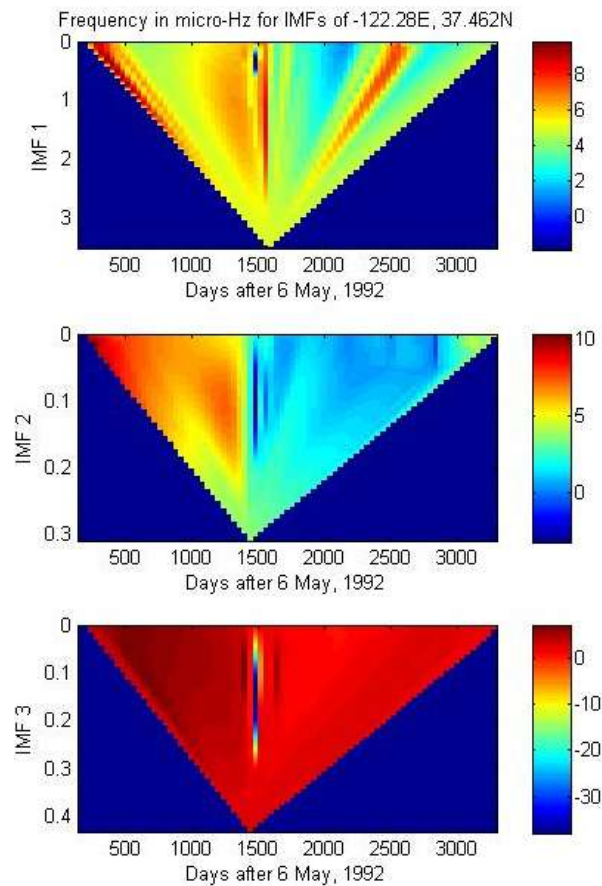


Figure 18c: Hilbert Spectrum for each of the IMFs extracted.

3.4 NETWORK INVERSION FILTER

The NIF as developed assumes knowledge of the mechanical source of deformation (generally fault slip as assumed in all applications of the method to date) and maps deformation data to time/space varying model parameters (slip rate and distribution). It tries to separate aspects in the data that appear to be due to the coherent contributions from this model from other time varying factors such as seasonal periodic and reference frame errors. The previous approaches directly explore the data for "real" time dependent components without knowledge or assumptions of what the underlying process is. We want to find "real" time dependent deformation features and resolve their spatio-temporal distribution as best as we can from a massive data set of noisy and sparse time series data.

4.1. Theory and use of Kalman Filtering

We model displacements at the Earth's surface $u_r(\mathbf{x}, t)$ as a function of spatial co-ordinate \mathbf{x} and time t by:

$$u_r(\mathbf{x}, t) = \int_{\Sigma} s_p(\boldsymbol{\xi}, t) G_{pq}^r(\mathbf{x}, \boldsymbol{\xi}) \mathbf{n}_q(\boldsymbol{\xi}) d\Sigma(\boldsymbol{\xi}) + \mathcal{L}(\mathbf{x}, t) + \epsilon. \quad (1)$$

The three terms on the right side of (1) represent the underlying deformation signal, local benchmark motion, and measurement error respectively. It is assumed that true deformation can be adequately represented by some spatially and temporally varying displacement discontinuity, or slip $s(\boldsymbol{\xi}, t)$ across one or more planar fault surfaces in a homogenous, isotropic, elastic half space. Deformation at depth below the seismogenic zone, may in fact be distributed across a fault zone of finite width, in which case the slip approximates the integrated strain across the fault. Although our focus here is on fault slip, opening mode sources (dikes) can be treated with the same procedure. We have not attempted to model distributed volume or pressure sources at this point. In (1) $p, q, r = 1, 2, 3$, summation on

repeated indices is implied, and $\mathbf{n}_q(\xi)$ is unit normal to the fault surface $\Sigma(\xi)$. The $G_{pq}(\mathbf{x}, \xi)$ derivatives of the elastostatic Green's tensors [e.g. Aki and Richards 1980]. We take the measurement errors to be normally distributed with a covariance matrix that is known (for example from the GPS data processing), at least to within a scalar factor σ^2 . There has been considerable discussion as to the appropriate stochastic model for local benchmark motions.

We take the local motions to be Brownian with scale parameter τ

$$B(t) = \tau \int_0^t d\mathbf{w}(t'), \quad (2)$$

Where $d\mathbf{w}$ is formal white noise. Note that τ^2 has unit *length² / time*. Other non-tectonic processes such as subsidence due to large scale fluid withdrawal or extensive landsliding, are not well modeled by random benchmark motions and should be treated separately. We take the estimated slip to be a linear combination of spatial functions $B(\mathbf{x})$:

$$s_p(\mathbf{x}, t) = \sum_{k=1}^M c_k^{(p)}(t) B_k(\mathbf{x}), \quad (3)$$

Where m is the number of basis functions included in the estimates. Substituting the model for slip (3) into (1) yields

$$u_r(\mathbf{x}_n, t) = \sum_{k=1}^M c_k^{(p)}(t) F_{rk}^{(p)} + \mathcal{L}(\mathbf{x}, t) + \epsilon, \quad (4)$$

$$F_{rk}^{(p)} \equiv \int_{\Sigma} B_k(\xi) C_{pq}^r(\mathbf{x}_n, \xi) \mathbf{n}_q(\xi) d\Sigma(\xi). \quad (5)$$

If the network contains n station with coordinates \mathbf{x}_n , $n=1,2,\dots,N$ the $3 \times N$ displacement components can be collected in a data vector \mathbf{d} ,

$$d_i(t_j) = u_r(\mathbf{x}_n, t_j), \quad i = 3(n-1) + r. \quad (6)$$

$$d_i(t_j) = \sum_{m=1}^{3M} c_m(t_j) F_{im} + \mathcal{L}_i(t_j) + \epsilon_{ij}. \quad (7)$$

$$\ddot{c}_m(t) = w_m(t), \quad (8)$$

Where $w_m(t)$ are independent white noise process with variance α^2 . \mathcal{L} here represents the seasonal parameters which can be removed according to prior analysis. Integrating (8) twice with respect to time yields:

$$c_m(t) = v_m t + W_m(t) \quad (9)$$

Where we assume without loss of generality that $c_m(t=0)=0$, that is, we measure accumulated slip from the time of the first observation. $W(t)$ is integrated random walk, with scale parameter α

$$W(t) = \int_0^t B(t') dt', \quad (10)$$

Where α^2 has unit of $length^2 / time^3$

3.4.2. Double Fault model for Loma Prieta

The 2 fault model proposed by *Burgmann et al* in 1997 required 2 dislocations to fit the data. The first corresponds to the Loma Prieta rupture and the second is a southwest dipping reverse thrust fault in the Foothills zone north of San Andreas. much of the deformation is best explained by relatively shallow sources above 15 km depth. Our preferred model involves contemporaneous oblique-slip and thrust faulting at high rates on two faults with similar strikes. The dip of the first fault is not tightly constrained and we can not clearly

differentiate if slip occurs on the SAF or the Loma Prieta rupture. However, we find that fault slip extends to very shallow depths, suggesting that faulting took place up-dip of the Loma Prieta fault. The inferred slip on the SAF or Loma Prieta fault may represent creep above, or between, the two high-slip asperities that released most of the earthquake moment [Beroza, 1991; Hartzell et al., 1991; Wald et al., 1991; Arnadottir and Segall, 1994; Horton, 1996]. The Foothills thrust belt has been active in the Quaternary and experienced shallow triggered slip during the Loma Prieta earthquake [Haugerud and Ellen, 1990; McLaughlin, 1990]. Our model thrust fault appears to coincide with the Berrocal fault zone, but it is possible that postseismic slip is distributed between several faults in this complex thrust system. Focal mechanisms of $M \geq 2.5$ Loma Prieta aftershocks, located NE of the SAF near the Berrocal fault zone, indicate that these events occurred predominantly on reverse faults (Figure 13). The seismicity near the Loma Prieta rupture on the other hand is very complex with all types of fault plane solutions [Oppenheimer, 1990; Beroza and Zoback, 1993].

3.4.3. Green's Function estimations

We use the equations in section 3.4.2 to estimate the slip on the 2 fault model. 'n' is the normal to the fault plane. L = random benchmark errors are estimated by the identification techniques discussed earlier. Since the transient phenomenon can be constrained and removed, what remains is the displacement due to the tectonic setting only. B are the Basis functions evaluated due to each fault patch for each slip direction, namely strike and dip. C is evaluated using random walk (discussed later) with parameter alpha, tau, sigma. To evaluate G or the green's functions, we use the code according to Okada 1985 for surface displacements due to tensile and shear faults in homogenous, elastic half space. 3 comp G at each of the PS ground data points is found, given the 2 fault model, due to each fault source discretized in patches. So, the motion is again resolved into a spatially varying term ($B \cdot G \cdot dA$: from the discretized fault patches + PS point positions) and a temporally varying term (C: from random walk components + data). For better resolution, we selected 12 as the number of basis functions for dip and strike slip. Hence total basis functions to be determined was

24 for each fault.. Also, each of the faults was discretized into a 12 by 7 grid, hence 168 fault elements in all. The results for the basis functions are shown in Figure 19.

3.4.4. Random Walk Model

This is a probabilistic estimation to determine the parameters alpha, gamma, tau and sigma that when fed into the network filter return the temporal factor C.

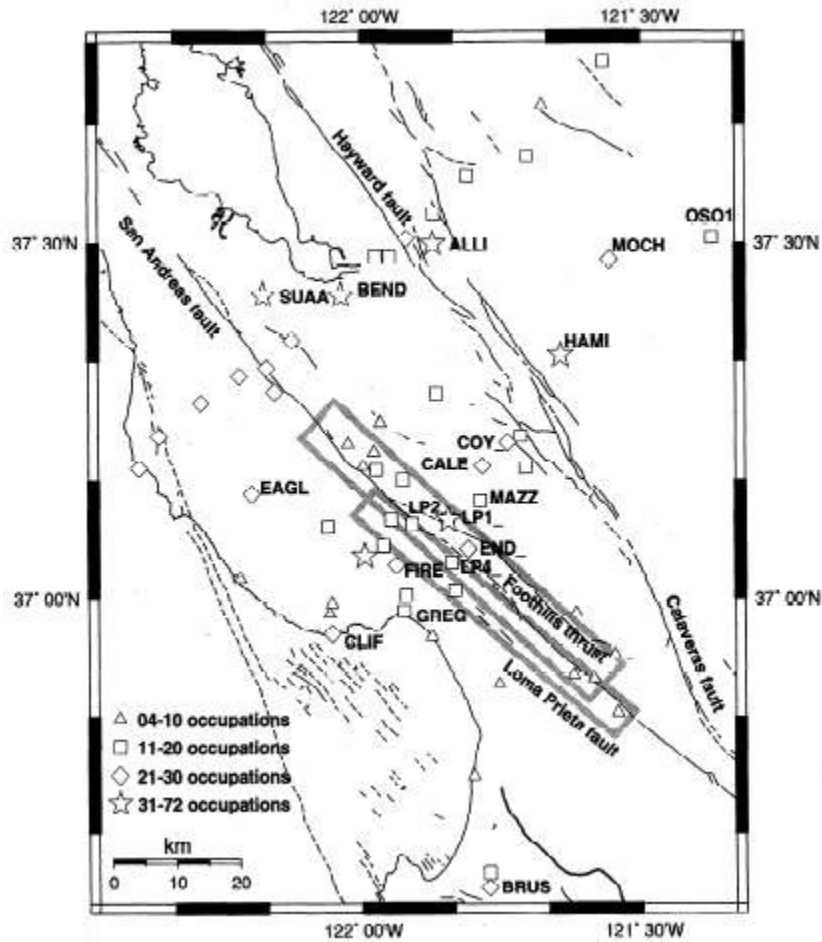


Figure 19: Two Fault Model for Loma Prieta proposed by Burgmann et al, 2000

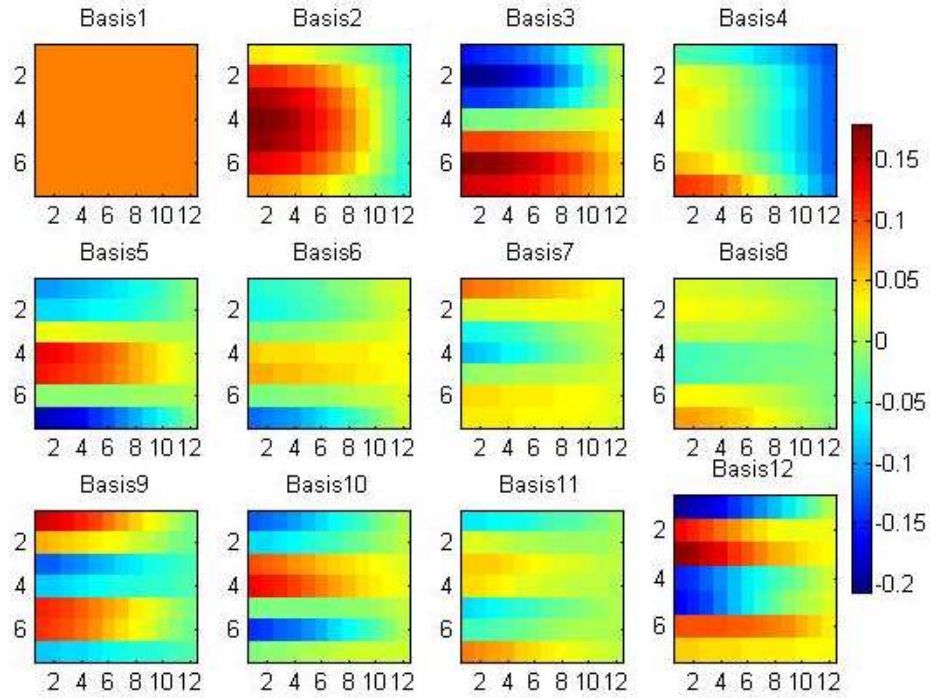


Figure 19a: 12 basis functions for the strike-slip part of Fault 1 discretized into 7 by 12 patches

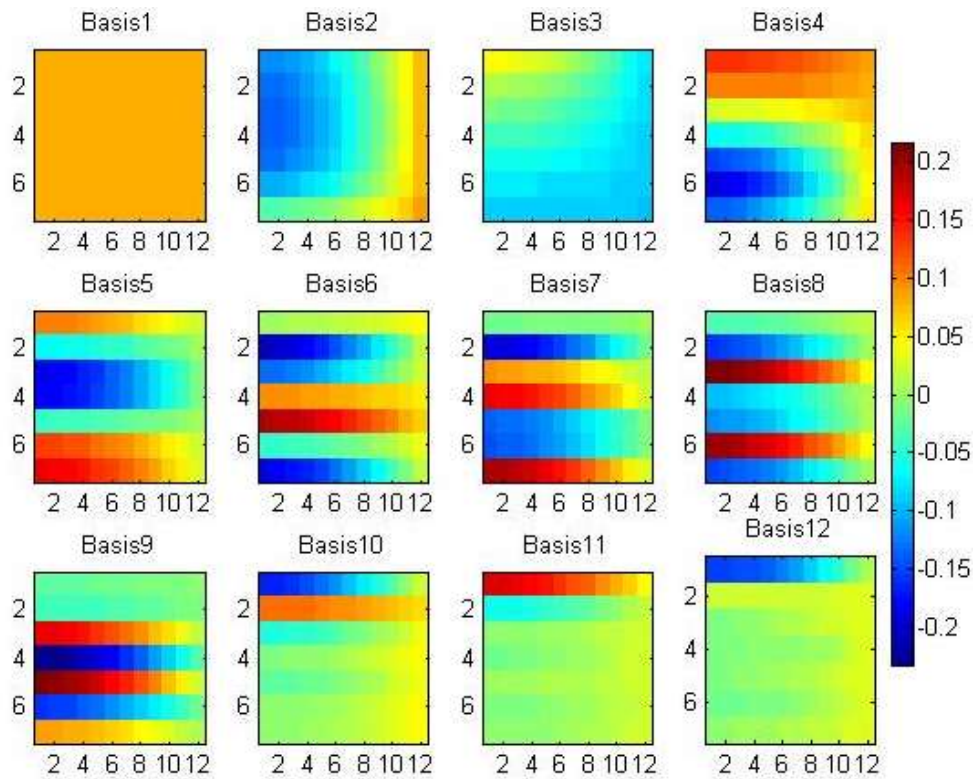


Figure 19b: 12 basis functions for the dip-slip part of Fault 1 discretized into 7 by 12 patches

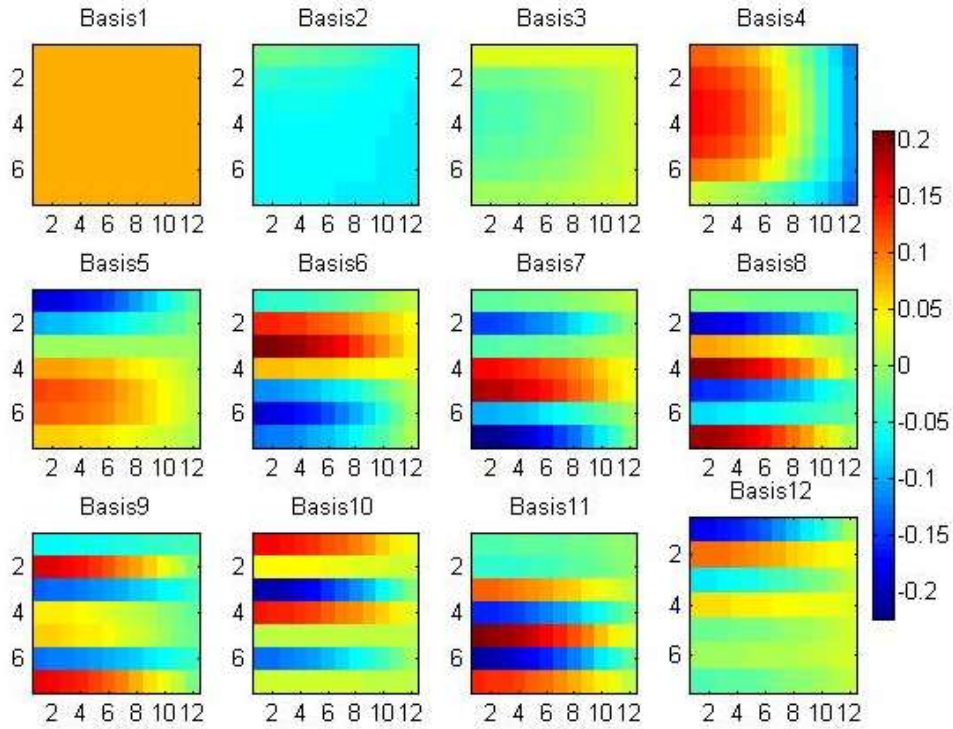


Figure 19c: 12 basis functions for the strike-slip part of Fault 2 discretized into 7 by 12 patches

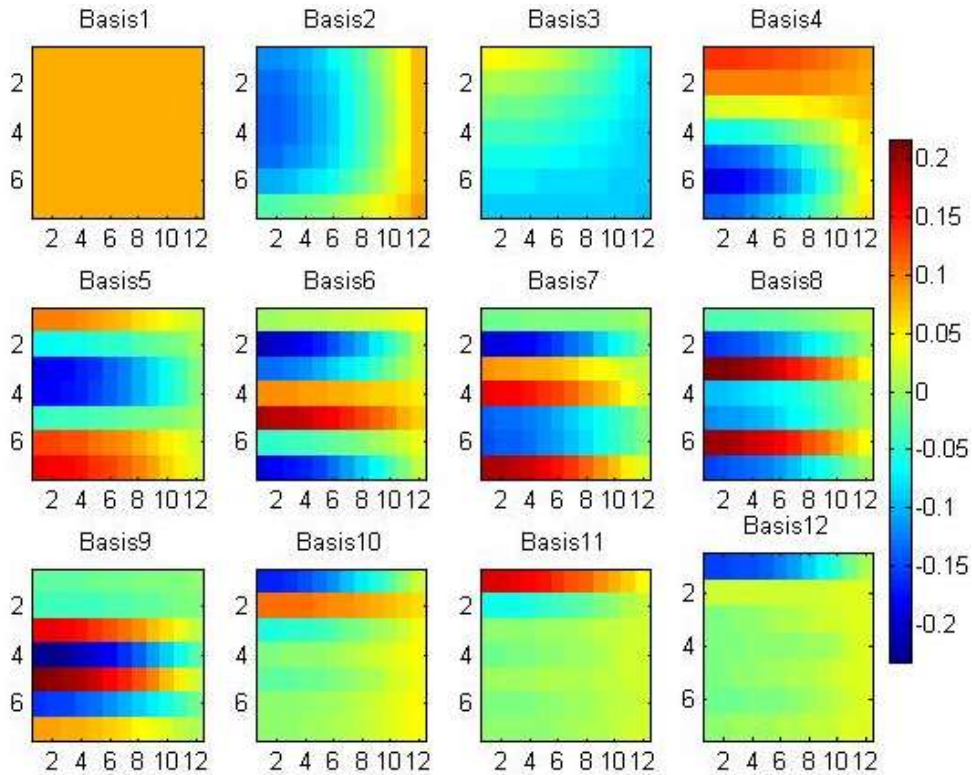


Figure 19d: 12 basis functions for the dip-slip part of Fault 2 discretized into 7 by 12 patches

The hyperparameters are determined via maximum likelihood method. Log likelihood is given by

$$\mathcal{L}(\Theta | \mathbf{d}_1, \dots, \mathbf{d}_{N_e}) = \sum_{k=1}^{N_e} \log[p_k(\mathbf{d}_k | \Theta; \mathbf{d}_1, \dots, \mathbf{d}_{k-1})]$$

Where The parameter vector Θ has components α^2 , σ^2 and τ^2 . The p_k on the RHS represents the probability density function (selected as the Gaussian in our case) such that the values on the LHS fit the given data. Iterating over random parameters in order to maximize likelihood or probability helps us thus find the parameters. First τ is determined as the value for which $-2*\log(\text{likelihood})$ becomes the minima. Using this value of τ , a contour plot of $-2*\log\text{likelihood}$ is made. The minimum valley in the plot indicates the value of α and Y for which it is obtained. σ has been normalized to 1 for simplicity purposes. The results are shown in Figure 20. Final values obtained are : $\tau = 0.02$, $\sigma = 1$, $\alpha = 3.54$, $Y = 7.24$. Log is taken in order to bring the pdf in product form:

$$p(\mathbf{d}_1, \dots, \mathbf{d}_{N_e} | \Theta) = \prod_{k=1}^{N_e} p_k(\mathbf{d}_k | \Theta; \mathbf{d}_1, \dots, \mathbf{d}_{k-1}).$$

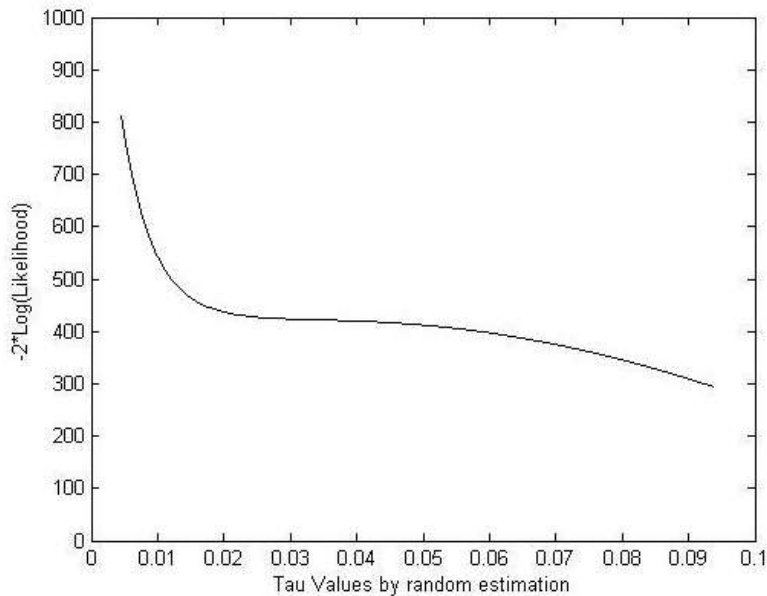


Figure 20a: Log Likelihood plot to determine tau.

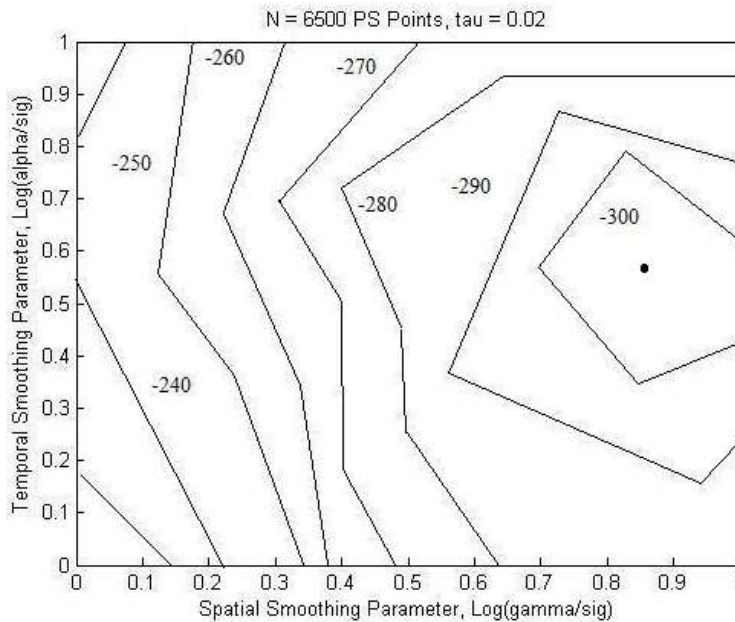


Figure 20b: $-2 \cdot \text{LogLikelihood}$ plot with respect to α , γ and σ after determining τ

3.4.5. Slip Estimation on Faults

Once the basis functions and C is found out as above, from the equations on section 3.4.1., slip rate can be estimated by a linear combination of the two at any epoch. To summarize, each of the basic vectors for a fault are multiplied with the time/epoch dependent parameter $c(i)$ where $I = \text{number of basis functions}$, and all the 24 contributions are summed to give the total slip on that fault. This is determined for each of the 168 fault patches. The entire algorithm is done once for the strike slip component and once for the dip slip component. The results are shown in Figure 21. The slip rate of the same region estimated by Network Inversion of GPS data in *Segall et al 2000* is shown in Figure 22. For Fault 1, the results show a significant match but for Fault 2, although the values are within the same order, the shape of the curves and the magnitude of error are high. The advantage of the kalman filter is that once the source is discretized into basis functions, the value of slip at any epoch can be determined by supplying new data from the stations, by a simple linear summation. In this project, we have downsampled the data continuously. Using the full dataset and if possible

more InSAR data could improve the results of slip. The inherent advantage of the Filter makes this modification convenient, given data.

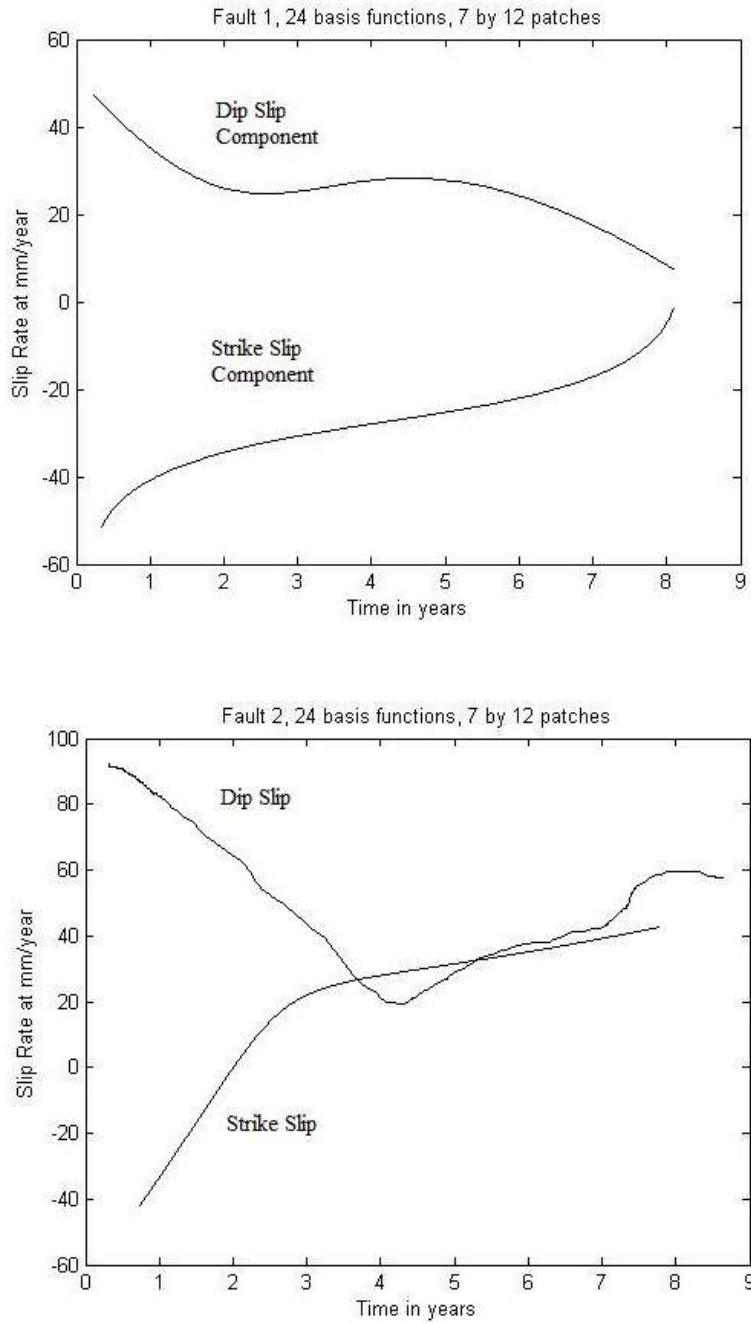


Figure 21a: Fault 1 slip parameter. Figure 21b: Fault 2 slip parameters

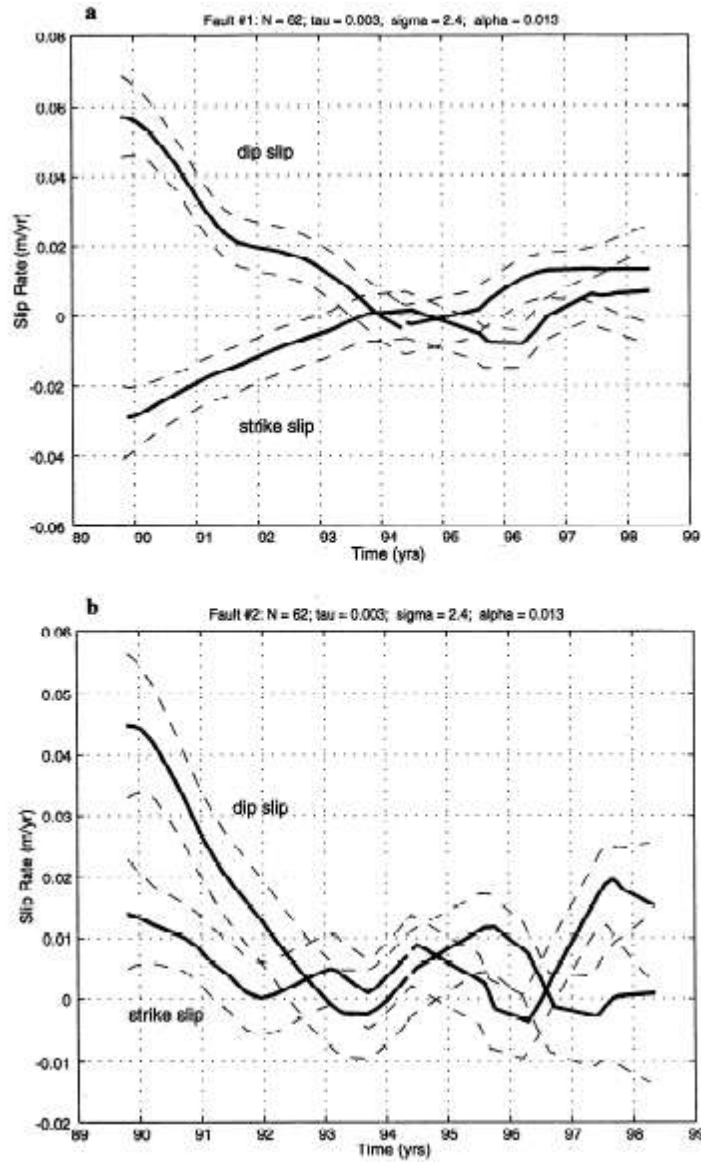


Figure 22: The slip model proposed by Segall et al 2000

3.5. SUMMARY AND DISCUSSION

Synthetic aperture radar interferometry is an imaging technique for measuring the topography of a surface, its changes over time, and other changes in the detailed characteristics of the surface. By exploiting the phase of the coherent radar signal, interferometry has transformed radar remote sensing from a largely interpretive science to a quantitative tool. Coherently combining the signals from two antennas, interferometric

phase difference between the received signals gives the geometric path length difference to the image point, which depends on the topography. Repeat pass over the same ground point at same antenna orientations give the surface displacement of that point over that period of time. The data is thus, time series of surface displacements of the San Francisco Bay Area and north across the Central Valley. We concentrated on (1) the time dependent land uplift/subsidence in the Santa Clara valley, California due to its strong seasonal character and (2) very slowly decaying late-stage postseismic relaxation in the Loma Prieta region since the 1989 earthquake.

Identification of the transients is done via functional fitting, Principal Component Analysis and Empirical Mode Decomposition. PCA at the Santa Clara region confirms that the NW-SE trending Silver Creek Fault divides the underlying aquifer into a region of subsidence and a region of uplift. For Loma Prieta, a total downthrow on the east of the San Andreas fault of three times the magnitude of upthrow on the west is calculated. The temporal factor shows a relaxation of the time series from 1993. In both cases, the first mode shows the maximum contribution and both match the GPS results obtained for the regions. Functional fitting confirms that Loma Prieta's signal is dominated by a logarithmic fit well above the sinusoidal and linear terms. The logarithmic relaxation period is calculated to be 4 years, which agrees with PCA. This can be explained by the viscous relaxation of a ductile (asthenospheric) layer underlying an elastic (lithospheric) plate. Functional fit on the west of the Silver Creek Fault showed uplift (mostly between 1995 and 1998) and on the west showed subsidence, both having very large coefficients of sinusoidal variation. This confirms the seasonal dominance of tectonics in the region. Previous work has attributed this phenomenon to inelastic deformation due to groundwater pumping and aquifer expansion. Lastly, EMD decomposes select traces into intrinsic mode functions by extracting the highest frequency signal, one at a time. This is applied to Santa Clara (due to its inferred seasonal character) and the Hilbert Amplitude Spectrum for the traces is made. The frequency content of each IMF, for each time sample, can thus be calculated for better evaluation of the seasonal character.

Modeling of the transients is done using the Network Inversion Filter. The NIF as developed assumes knowledge of the mechanical source of deformation and maps deformation data to time/space varying model parameters (slip rate and distribution). It tries to separate aspects in the data that appear to be due to the coherent contributions from this model from other time varying factors such as seasonal periodic and reference frame errors. The Loma Prieta region is modeled using a 2 fault model inverted from GPS data. The slip on the fault is resolved into a spatially varying term (Basis and Green's functions from the discretized fault patches and PS point positions) and a temporally varying term (from random walk components and data-dependent). The filter hyperparameters are determined by the maximum likelihood technique and the final slip calculated compared with previous GPS results.

InSAR is thus a very powerful tool to examine transient, slowly varying processes such as creeps, volcanic deformations, subsidence and seismic relaxations. Mathematical techniques applied to two such processes near the San Andreas fault have been studied and compared.